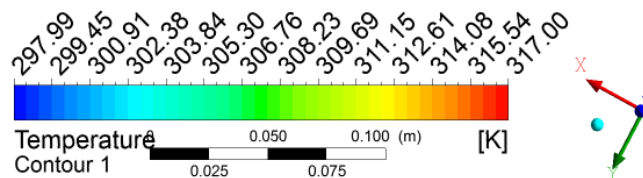


CHALMERS



Heat Transfer Optimization of Shell-and-Tube Heat Exchanger through CFD Studies

Master's Thesis in Innovative and Sustainable Chemical Engineering

USMAN UR REHMAN

Department of Chemical and Biological Engineering
Division of Chemical Engineering
CHALMERS UNIVERSITY OF TECHNOLOGY
Göteborg, Sweden 2011
Master's Thesis 2011:09

MASTER'S THESIS 2011:09

Heat Transfer Optimization of Shell-and-Tube Heat Exchanger through CFD Studies

Master's Thesis in Innovative and Sustainable Chemical Engineering
USMAN UR REHMAN

Department of Chemical and Biological Engineering
Division of Chemical Engineering
CHALMERS UNIVERSITY OF TECHNOLOGY

Göteborg, Sweden 2011

Heat Transfer Optimization of Shell-and-Tube Heat Exchanger through CFD Studies
USMAN UR REHMAN

©USMAN UR REHMAN, 2011

Master's Thesis 2011:09

ISSN xxxx-xxxx

Supervisor: Ronnie Andersson PhD

Examiner: Professor Bengt Andersson

”The work is done with the collaboration of TetraPak Processing Systems (Lund, Sweden)”

Department of Chemical and Biological Engineering

Division of Chemical Engineering

Chalmers University of Technology

SE-412 96 Göteborg

Sweden

Telephone: + 46 (0)722687465

Cover:

Contour Plot of Temperature distribuion on the Tube walls

Chalmers Reproservice

Göteborg, Sweden 2011

Preface

In this study the design and simulation of an industrial scale TetraPak shell and tube heat exchanger was carried out. The current design has been evaluated in the light of Computational Fluid Dynamics (CFD) studies. The work has been carried out from May 2011 to September 2011 at the Department of Chemical and Biological Engineering,, Chalmers University of Technology, Sweden, with Usman ur Rehman as student and Professor Dr. Bengt Andersson and Ronnie Andersson as supervisors.

Göteborg Sep 2011
Usman ur Rehman

Acknowledgement

After the several months of work, it took to produce the few pages before you, a few people that were support to this project need to be thanked. First and most of all Prof.Dr. **Bengt Andersson**, for his supervision of the project and freedom he left for me to choose most of the project direction and working hours. Secondly, Dr. **Ronnie Andersson** was always there to help and without his guidance this project was never going to find an end. I would like to thank Dr. **Fredrik Innings** at TetraPak, who gave me the opportunity to work on this project and helped to get industrial experience as well. Thanks to everybody around in Master Thesis room, who has always provided a perfect environment for the research and development at all levels.

For support to the project I would also like to thank Arash and Yaseen for always encouraging me and sharing some memorable time , specially at coffee breaks. Special thanks to my friends , Saqib, Waqar and Usman for motivating me and always helping me in any kind of problem. It was no doubt some great time here and would always remember the moments I spent here.

Göteborg Sep 2011
Usman ur Rehman

Abstract

An un-baffled shell-and-tube heat exchanger design with respect to heat transfer coefficient and pressure drop is investigated by numerically modeling. The heat exchanger contained 19 tubes inside a 5.85m long and 108mm diameter shell. The flow and temperature fields inside the shell and tubes are resolved using a commercial CFD package considering the plane symmetry. A set of CFD simulations is performed for a single shell and tube bundle and is compared with the experimental results. The results are found to be sensitive to turbulence model and wall treatment method. It is found that there are regions of low Reynolds number in the core of heat exchanger shell. Thus, $k-\omega$ SST model, with low Reynolds correction, provides better results as compared to other models. The temperature and velocity profiles are examined in detail. It is seen that the flow remains parallel to the tubes thus limiting the heat transfer. Approximately, 2/3rd of the shell side fluid is bypassing the tubes and contributing little to the overall heat transfer. Significant fraction of total shell side pressure drop is found at inlet and outlet regions. Due to the parallel flow and low mass flux in the core of heat exchanger, the tubes are not uniformly heated. Outer tubes fluid tends to leave at a higher temperature compared to inner tubes fluid. Higher heat flux is observed at shell's inlet due to two reasons. Firstly due to the cross-flow and secondly due to higher temperature difference between tubes and shell side fluid. On the basis of these findings, current design needs modifications to improve heat transfer. Keywords: Heat transfer, Shell-and-Tube Heat exchanger, CFD, Un-baffled

Contents

Preface	I
Acknowledgments	II
Abstract	III
Contents	V
List of Tables	VII
List of Figures	VIII
1 Introduction	1
1.1 Background	1
1.1.1 Heat Exchanger Classification	1
1.1.2 Applications of Heat exchangers	2
1.2 Literature Survey	2
1.3 Tubular Heat Exchanger	4
1.3.1 Heat Transfer	4
1.3.2 Overall Heat Transfer Coefficient	6
2 Mathematical background and CFD	7
2.1 Flow Calculation	7
2.1.1 Continuity Equation	7
2.1.2 Momentum Equations (Navier-Stokes Equations)	7
2.1.3 Energy Equation	8
2.2 Turbulence Modeling	9
2.2.1 Turbulence Model	9
2.2.2 Two-Equations Models	10
2.3 Wall Treatment Methods	13
2.3.1 Wall Functions	13
3 CFD Analysis	19
3.1 Geometry	19
3.2 Mesh	20
3.2.1 y^+ Values	20
3.2.2 Grid Independence	20
3.3 Solution	23
3.3.1 Boundary Conditions	23
3.3.2 Discretization Scheme	24
3.3.3 Measure of Convergence	24
4 Results and Discussion	25
4.1 Model Comparison	25
4.2 CFD Comparison with Experimental Results	26
4.3 Contour Plots	27

4.4	Vector Plots	30
4.5	Profiles	30
4.5.1	Velocity Profile	31
4.5.2	Temperature Profiles	32
4.6	Mass and Heat Flux	34
4.7	Pressure Drop and Heat Transfer	35
5	Conclusions	37
	Bibliography	38

List of Tables

1.1	Heat Exchanger Applications in Different Industries	2
2.1	Closure Coefficients for $k - \varepsilon$ Model	11
2.2	Closure Coefficients for $k - \omega$ Model	12
3.1	Heat Exchanger Dimensions	20
3.2	Different Meshes	21
3.3	y^+ Values for Different Wall Treatments	22
3.4	Boundary Conditions	24
3.5	Residuals	24
4.1	Velocity and Temperature Contour Plots	29

List of Figures

1.1	Counter-current Heat Exchanger Arrangement (<i>Courtesy Washington University</i>)	1
1.2	Heat Transfer in a Heat Exchanger adopted from “Heat Transfer in Process Engineering(2009)”	5
2.1	Wall Functions and Near Wall Treatment (Adopted from ”Computational Fluid Dynamics for Chemical Engineers”)	14
2.2	The Law of Wall (Adopted from ”Computational Fluid Dynamics for Chemical Engineers”)	15
3.1	Geometry	19
3.2	Mesh Composition	22
3.3	Velocity Profiles for Different Meshes	23
3.4	Temperature Profiles for Different Meshes	23
4.1	Over all Heat Transfer Coefficient	25
4.2	Pressure Drop	25
4.3	CFD and Experimental Results	26
4.4	Comparison of Shell Side Pressure Drop	27
4.5	Comparison of Tube Side Pressure Drop	27
4.6	Comparison of Overall Heat Transfer Coefficient	27
4.7	Velocity Contour Plot at Symmetrical Plane	28
4.8	Temperature Contour Plot at Symmetrical Plane	28
4.9	Vector Plot of Velocity at Inlet	30
4.10	Vector Plots	30
4.11	Profiling	31
4.12	Velocity Profiles Across the Cross-section at Different Positions in the Heat Exchanger	32
4.13	Temperature Profiles Across the Cross-section at Different Positions in the Heat Exchanger	33
4.14	Tube side Temperature Profiles along the Length of Heat Exchanger	33
4.15	Mass Averaged Shell and Tube side Temperatures	34
4.16	Shell and Tube Side Temperature Profiles along the Length of Heat Exchanger	34
4.17	Contour Plots	35
4.18	Shell Side Pressure Drop along the Length of Heat Exchanger	36
4.19	Heat Transfer Coefficient along the Length of Heat Exchanger	36

Chapter 1

Introduction

1.1 Background

Heat exchangers are one of the mostly used equipments in the process industries. Heat exchangers are used to transfer heat between two process streams. One can realize their usage that any process which involves cooling, heating, condensation, boiling or evaporation will require a heat exchanger for these purposes. Process fluids, usually are heated or cooled before the process or undergo a phase change. Different heat exchangers are named according to their applications. For example, heat exchangers being used to condense are known as condensers, similarly heat exchangers for boiling purposes are called boilers. Performance and efficiency of heat exchangers are measured through the amount of heat transferred using least area of heat transfer and pressure drop. A more better presentation of its efficiency is done by calculating over all heat transfer coefficient. Pressure drop and area required for a certain amount of heat transfer, provides an insight about the capital cost and power requirements (Running cost) of a heat exchanger. Usually, there is lots of literature and theories to design a heat exchanger according to the requirements. A good design is referred to a heat exchanger with least possible area and pressure drop to fulfill the heat transfer requirements[1].

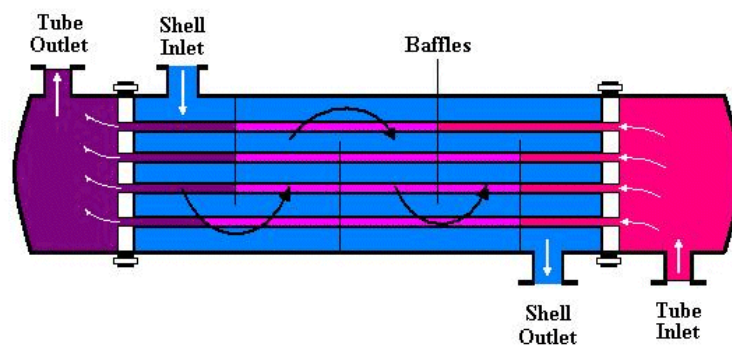


Figure 1.1: Counter-current Heat Exchanger Arrangement (Courtesy Washington University)

1.1.1 Heat Exchanger Classification

At present heat exchangers are available in many configurations. Depending upon their application, process fluids, and mode of heat transfer and flow, heat exchangers can be classified[2].

Heat exchangers can transfer heat through direct contact with the fluid or through indirect ways. They can also be classified on the basis of shell and tube passes, types of baffles, arrangement of tubes (Triangular, square etc.) and smooth or baffled surfaces. These are also classified

through flow arrangements as fluids can be flowing in same direction(Parallel), opposite to each other (Counter flow) and normal to each other (Cross flow). The selection of a particular heat exchanger configuration depends on several factors. These factors may include, the area requirements, maintenance, flow rates, and fluid phase.

1.1.2 Applications of Heat exchangers

Applications of heat exchangers is a very vast topic and would require a separate thorough study to cover each aspect. Among the common applications are their use in process industry, mechanical equipments industry and home appliances. Heat exchangers can be found employed for heating district systems, largely being used now a days. Air conditioners and refrigerators also install the heat exchangers to condense or evaporate the fluid. Moreover, these are also being used in milk processing units for the sake of pasteurization. The more detailed applications of the heat exchangers can be found in the Table 1.1 w.r.t different industries[3].

Table 1.1: Heat Exchanger Applications in Different Industries

Industries	Applications
Food and Beverages	Ovens, cookers, Food processing and pre-heating, Milk pasteurization, beer cooling and pasteurization, juices and syrup pasteurization, cooling or chilling the final product to desired temperatures.
Petroleum	Brine cooling, crude oil pre-heating, crude oil heat treatment, Fluid interchanger cooling, acid gas condenser.
Hydro carbon processing	Preheating of methanol, liquid hydrocarbon product cooling, feed pre-heaters, Recovery or removal of carbon dioxide, production of ammonia.
Polymer	Production of polypropylene, Reactor jacket cooling for the production of polyvinyl chloride.
Pharmaceutical	Purification of water and steam, For point of use cooling on Water For Injection ring.
Automotive	Pickling, Rinsing, Priming, Painting.
Power	Cooling circuit, Radiators, Oil coolers, air conditioners and heaters, energy recovery.
Marine	Marine cooling systems, Fresh water distiller, Diesel fuel pre-heating, central cooling, Cooling of lubrication oil.

1.2 Literature Survey

Shell and tube heat exchanger design is normally based on correlations, among these, the Kern method [4] and Bell-Delaware method [5] are the most commonly used correlations. Kern method is mostly used for the preliminary design and provides conservative results. Whereas, the Bell-Delaware method is more accurate method and can provide detailed results. It can predict and estimate pressure drop and heat transfer coefficient with better accuracy. The Bell-Delaware method is actually the rating method and it can suggest the weaknesses in the shell side design but it cannot indicate where these weaknesses are. Thus in order to figure out these problems, flow distribution must be understood. For this reason, several analytical, experimental and numerical studies have been carried out. Most of this research was concentrated on the certain aspects of the shell and tube heat exchanger design[6]. These correlations are developed for baffled shell and

tube heat exchangers generally. Our studies aims at studying simple un-baffled heat exchanger, which is more similar to the double pipe heat exchangers. Almost no studies is found for an un-baffled shell and tube heat exchanger. Thus general correlations of heat transfer and pressure drop for straight pipes can be useful to get an idea of the design. Generally there has been lot of work done on heat transfer [7] and pressure drop[8] in heat exchangers. Pressure drop in a heat exchanger can be divided in three parts. Mainly it occurs due to fanning friction along the pipe. In addition to this it also occurs due to geometrical changes in the flow i.e. contraction and expansion at inlet and outlet of heat exchanger [9]. Handbook of hydraulic resistance provides the correlations for the pressure losses in these three regions separately by introducing the pressure loss coefficients. Entrance and exit losses are calculated by the equations 1.1 and 1.2 respectively.

$$\Delta P_{en} = (1 - \sigma_e^2 + K_c) \frac{G^2}{2\rho} \quad (1.1)$$

$$\Delta P_{ex} = -(1 - \sigma_e^2 - K_e) \frac{G^2}{2\rho} \quad (1.2)$$

Where,

G = Mass velocity (kg/m^2s)

σ = Minimum Flow area / Frontal area = A_1/A_2

K_c = Entrance pressure drop coefficient

K_e = Exit pressure drop coefficient

As the heat exchanger under our study is un-baffled, thus making it similar to the straight annular pipe. Pressure drop in the shell side except the inlet and outlet regions can be estimated by considering the hydraulic diameter of the heat exchanger [9] and using Darcy–Weisbach equation.

$$\Delta P = f \frac{L\rho v^2}{2D} \quad (1.3)$$

Where,

ΔP = Pressure drop (Pa)

f = Fanning friction factor

L = Length of pipe (m)

ρ = Fluid density (kg/m^3)

D = Hydraulic diameter of pipe (m)

Similarly, heat transfer coefficient can also be estimated as for an annular pipe [10]. Meyer et al has validated a CFD model of a three dimensional tube-in-tube heat exchanger [10]. It used a Dittus-Boelter correlation to compare the heat transfer coefficient with CFD results. Dittus-Boelter correlation as in equation 1.4 provides Nusselt number by the help of Reynolds and Prandtl number.

$$Nu = 0.023Re^{0.8}Pr^n \quad (1.4)$$

Compared to correlation based methods, the use of CFD in heat exchanger design is limited. CFD can be used both in the rating, and iteratively in the sizing of heat exchangers. It can be particularly useful in the initial design steps, reducing the number of tested prototypes and providing a good insight in the transport phenomena occurring in the heat exchangers[11]. To be able to run a successful full CFD simulation for a detailed heat exchanger model, large amounts of computing power and computer memory as well as long computation times are required. Without any simplification, an industrial shell and tube heat exchanger with 500 tubes and 10 baffles would require at least 150 million computational elements, to resolve the geometry[12]. It is not possible to model such geometry by using an ordinary computer. To overcome that difficulty, in the previous works, large scale shell-and-tube heat exchangers are modeled by using

some simplifications. The commonly used simplifications are the porous medium model and the distributed resistance approach. Shell-and-tube heat exchangers can be modeled using distributed resistance approach[12]. By using this method, a single computational cell may have multiple tubes; therefore, shell side of the heat exchanger can be modeled by relatively coarse grid. Kao et al [13] developed a multidimensional, thermal-hydraulic model in which shell side was modeled using volumetric porosity, surface permeability and distributed resistance methods. In all of these simplified approaches, the shell side pressure drop and heat transfer rate results showed good agreement with experimental data.

With the simplified approaches, one can predict the shell side heat transfer coefficient and pressure drop successfully, however for visualization of the shell side flow and temperature fields in detail, a full CFD model of the shell side is needed. With ever increasing computational capabilities, the number of cells that can be used in a CFD model is increasing. Now it is possible to model an industrial scale shell- and-tube heat exchanger in detail with the available computers and softwares. By modeling the geometry as accurately as possible, the flow structure and the temperature distribution inside the shell can be obtained. This detailed data can be used for calculating global parameters such as heat transfer coefficient and pressure drop that can be compared with the correlation based or experimental ones[6]. Moreover, the data can also be used for visualizing the flow and temperature fields which can help to locate the weaknesses in the design such as recirculation and re-laminarization zones.

According to a recent review [14], commercial and non commercial softwares are used to model different types of heat exchangers. Normally, for modeling the flow, two equation models are the most commonly used models. $k - \epsilon$ models are mostly used in industrial designs along with wall functions. Jae et al [15] compared the different near wall treatment methods for high Reynolds number flows. It was found that non-equilibrium wall functions along with $k - \epsilon$ models predicts the reattachment lengths more accurately, but two layer model represents the overall flow domain much better. The use of these near wall treatments is very much dependent upon the choice of turbulence model used.

1.3 Tubular Heat Exchanger

1.3.1 Heat Transfer

Heat transfer is considered to be the basic process of all process industries. During the process of heat transfer, one fluid at higher temperature transfers its energy in the form of heat to the other fluid at a lower temperature. Fluid can transfer its heat through different mechanisms. These mechanisms of heat transfer are conduction, convection and radiation. Radiation is not so common mode of heat transfer in process industries but in some processes it plays a vital role in heat transfer for example in combustion furnace. Other two modes of heat transfer i.e conduction and convection are most encountered modes of heat transfer in process industries[16][4].

Overall energy balance of a heat transfer system can be generalized by the Equations 1.5 and 1.6.

$$Q_h = m_h C_p (T_{h,i} - T_{h,o}) \quad (1.5)$$

$$Q_c = m_c C_p (T_{c,o} - T_{c,i}) \quad (1.6)$$

In actual heat provided by a hotter fluid to the fluid at low temperature is not exactly equal due to losses and resistances in the form of wall fouling. Assumption is made that the amount of heat transferred from the hotter fluid is equal to the amount of heat transferred to the colder fluid. Usually, heat exchangers are made isolated to minimize the environmental losses. So we can write as under,

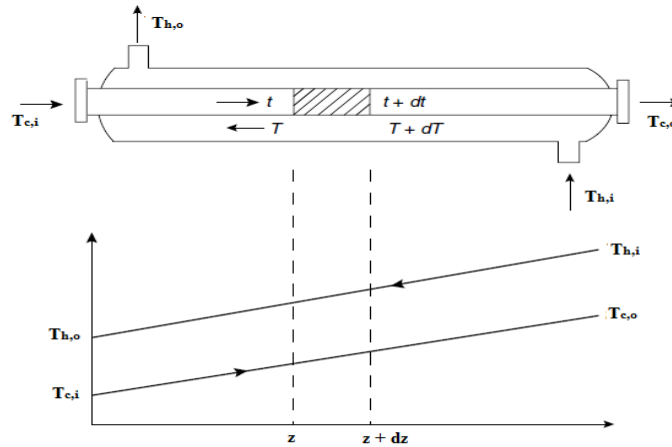


Figure 1.2: Heat Transfer in a Heat Exchanger adopted from “Heat Transfer in Process Engineering(2009)“

$$Q_h = Q_c = Q$$

Graphical representation of these equations makes the process easier and simplified to understand. These graphs are known as T-Q diagrams. These graphs also helps in making sure that 2nd law of thermodynamics is obeyed i.e heat should always be transferred from higher temperature to lower temperature.

Then we can write the Equations in the form,

$$Q = UA\Delta T_{LM} \tag{1.7}$$

Where,

Q = Heat transfer rate (W)

A = Heat transfer area (m^2)

U = Overall heat transfer coefficient ($W/m^2.K$)

ΔT_{LM} = Logarithmic mean temperature difference (K)

These three equations 1.5 to 1.7 are considered to be the fundamental equations for all heat transfer problems.

These equations are derived by the help of different assumptions. Mainly, the overall heat transfer coefficient and specific heat capacity are considered constant for the heat exchangers. In real practice, these values can change depending upon the fluids properties and temperatures. It is observed that specific heat capacity of many industrial fluids such as water, remains constant for a range of temperatures. For example,

Specific heat capacity of water at 273.5K and atmospheric pressure = 4218 J/kg.K

Specific heat capacity of water at 374K and atmospheric pressure = 4226 J/kg.K

Thus we can say that this assumption works well for such temperature ranges. Specific heat of a fluid is the property of fluid by which it transfers heat. In other words, it is the amount of heat needed by the one kilogram of fluid to raise its temperature by one degree Celsius. The log mean temperature difference (LMTD) is calculated to estimate the average temperature difference throughout the heat exchanger. It is basically the logarithmic average of temperature difference. As for a heat transfer the driving force is always the temperature difference, thus higher log mean temperature difference will ensure better heat transfer. It is related to area of

heat exchanger in a way that higher LMTD will cause less heat transfer area and lower LMTD will need larger heat transfer area. Generally, LMTD is a process condition and one cannot do much about it as inlet and outlet temperatures of fluids are usually pre decided for a heat exchanger design. Area can certainly be reduced by making the full use of available LMTD by efficient heat transfer.

1.3.2 Overall Heat Transfer Coefficient

The overall heat transfer of heat exchangers is the ability of transferring heat through different resistances, It depends upon, the properties of the process fluids, temperatures, flow rates and geometrical arrangement of the heat exchanger. For example, the number of passes, number of baffles and baffle spacing etc. It is defined by the Equation 1.8. This equation basically sums up all the resistances encountered during the heat transfer and taking the reciprocal gives us the overall heat transfer coefficient[16].

$$\frac{1}{U} = \frac{1}{h_h} + \frac{\Delta x}{k} + \frac{1}{h_c} + R_f \quad (1.8)$$

Where:

h_h = Hot side heat transfer coefficient ($W/m^2.K$)

h_c = Cold side heat transfer coefficient ($W/m^2.K$)

Δx = Exchanger tube wall thickness (m)

k = Exchanger wall material thermal conductivity ($W/m.K$)

R_f = Fouling coefficient ($W/m^2.K$) The equation for the overall heat transfer coefficient can be written as the equation 1.9.

$$\frac{1}{U} = \frac{1}{h_h} + \frac{1}{h_c} + R_f \quad (1.9)$$

h_h and h_c are the individual film coefficients and are defined as the measure of heat transfer for unit area and unit temperature difference. These are calculated separately for both outside and inside fluids. The temperature difference of average temperature of bulk fluid (hot and cold) and wall temperature (inside and outside) is the driving force for the respective fluids. $\Delta x/k$ is usually ignored as it doesn't have a significant effect on the over all heat transfer coefficient.[16].

Chapter 2

Mathematical background and CFD

In this chapter, the governing equations solved by FLUENT and the turbulence models used for this simulation are explained. Two equation models are used for the simulations. Flow equations and energy equations are described in detail. The wall treatment methods are also discussed and how they are important for modeling the heat transfer is also described.

2.1 Flow Calculation

The flow is governed by the continuity equation, the energy equation and Navier-Stokes momentum equations. Transport of mass, energy and momentum occur through convective flow and diffusion of molecules and turbulent eddies. All equations are set up over a control volume where $i, j, k = 1, 2, 3$ correspond to the three dimensions[17].

2.1.1 Continuity Equation

The continuity equation describes the conservation of mass and is written as in equation

$$\frac{\partial \rho}{\partial t} + \frac{\partial \rho U_1}{\partial x_1} + \frac{\partial \rho U_2}{\partial x_2} + \frac{\partial \rho U_3}{\partial x_3} = 0 \quad (2.1)$$

or

$$\frac{\partial \rho}{\partial t} + \frac{\partial \rho U_i}{\partial x_i} = 0, i = 1, 2, 3$$

Equation 2.1 defines the rate of increase of mass in a control volume as equal to the amount through its faces. Whereas, for constant density continuity equation is reduced to

$$\frac{\partial U_i}{\partial x_i} = 0, i = 1, 2, 3$$

2.1.2 Momentum Equations (Navier-Stokes Equations)

The momentum balance, also known as the Navier-Stokes equations, follows Newton's second law: The change in momentum in all directions equals the sum of forces acting in those directions. There are two different kinds of forces acting on a finite volume element, surface forces and body forces. Surface forces include pressure and viscous forces and body forces include gravity, centrifugal and electro-magnetic forces[17].

The momentum equation in tensor notation for a Newtonian fluid can be written as in equation 2.2

$$\frac{\partial U_i}{\partial t} + U_j \frac{\partial U_i}{\partial x_j} = -\frac{1}{\rho} \frac{\partial P}{\partial x_i} + \nu \frac{\partial}{\partial x_j} \left(\frac{\partial U_i}{\partial x_j} + \frac{\partial U_j}{\partial x_i} \right) + g_i \quad (2.2)$$

The equation 2.2 can be written in different forms for constant density and viscosity since $\nu \frac{\partial}{\partial x_j} \left(\frac{\partial U_i}{\partial x_j} + \frac{\partial U_j}{\partial x_i} \right) = \nu \frac{\partial^2 U_i}{\partial x_j \partial x_i}$ in incompressible flow. In addition to gravity, there can be further external sources that may effect the acceleration of fluid e.g. electrical and magnetic fields. Strictly it is the momentum equations that form the Navier-Stokes equations but sometimes the continuity and momentum equations together are called the Navier-Stokes equations. The Navier-Stokes equations are limited to macroscopic conditions.[17].

The continuity equation is difficult to solve numerically. In CFD programs, the continuity equation is often combined with momentum equation to form Poisson equation 2.3. For constant density and viscosity the new equation can be written as below.

$$\frac{\partial}{\partial x_i} \left(\frac{\partial P}{\partial x_i} \right) = -\frac{\partial}{\partial x_i} \left(\frac{\partial(\rho U_i U_j)}{\partial x_j} \right) \quad (2.3)$$

This equation has more suitable numerical properties and can be solved by proper iteration methods.

2.1.3 Energy Equation

Energy is present in many forms in flow i.e. as kinetic energy due to the mass and velocity of the fluid, as thermal energy, and as chemically bounded energy. Thus the total energy can be defined as the sum of all these energies[17].

$$h = h_m + h_T + h_C + \Phi \quad (2.4)$$

$h_m = \frac{1}{2} \rho U_i U_i$	Kinetic energy
$h_T = \sum_n m_n \int_{T_{ref}}^T C_{p,n} dT$	Thermal energy
$h_C = \sum_n m_n h_n$	Chemical energy
$\Phi = g_i x_i$	Potential energy

In the above equations m_n and $C_{p,n}$ are the mass fraction and specific heat for species n. The transport equation for total energy can be written by the help of above equations. The coupling between energy equations and momentum equations is very weak for incompressible flows, thus equations for kinetic and thermal energies can be written separately. The chemical energy is not included because there was no species transport involved in this project.

The transport equation for kinetic energy can be written as under,

$$\frac{\partial(h_m)}{\partial t} = -U_j \frac{\partial(h_m)}{\partial x_j} + P \frac{\partial U_i}{\partial x_i} - \frac{\partial(P U_i)}{\partial x_i} - \frac{\partial}{\partial x_j} (\tau_{ij} U_i) - \tau_{ij} \frac{\partial U_i}{\partial x_j} + \rho g U_i \quad (2.5)$$

The last term in the equation 2.5 is the work done by the gravity force. Similarly, a balance for heat can be formulated generally by simply adding the source terms from the kinetic energy equation.

$$\frac{\partial(\rho C_p T)}{\partial t} = -U_j \frac{\partial(\rho C_p T)}{\partial x_j} + k_{eff} \frac{\partial^2 T}{\partial x_j \partial x_j} - P \frac{\partial U_j}{\partial x_j} + \tau_{kj} \frac{\partial U_k}{\partial x_j} \quad (2.6)$$

The term on left side of the equation is accumulation term. The first on the right is convection term, second is the conduction, third expansion and last is dissipation term. Here the terms in the equation for transformation between thermal and kinetic energy, i.e. expansion and dissipation occur as source terms.

2.2 Turbulence Modeling

Definition of Turbulence

Turbulent flows have some characteristic properties which distinct them from laminar flows[17].

- The motions of the fluid in a turbulent flow are irregular and chaotic due to random movements by the fluid. The flow has a wide range of length, velocity and time scales.
- Turbulence is a three dimensional diffusive transport of mass, momentum and energy through the turbulent eddies that result in faster mixing rates.
- Energy has to be constantly supplied or the turbulent eddies will decay and the flow will become laminar, the kinetic energy becomes internal energy.

Turbulence arises due to the instability in the flow. This happens when the viscous dampening of the velocity fluctuations is slower than the convective transport, i.e. the fluid element can rotate before it comes in contact with wall that stops the rotation. For high Reynolds numbers the velocity fluctuations cannot be dampened by the viscous forces and the flow becomes turbulent.

Turbulent flows contain a wide range of length, velocity and time scales and solving all of them makes the costs of simulations large. Therefore, several turbulence models have been developed with different degrees of resolution. All turbulence models have made approximations simplifying the Navier-Stokes equations. There are several turbulence models available in CFD-software including the Large Eddy Simulation (LES) and Reynolds Average Navier-Stokes (RANS). There are several RANS models available depending on the characteristic of flow, e.g., Standard $k - \varepsilon$ model, $k - \varepsilon$ RNG model, Realizable $k - \varepsilon$, $k - \omega$ and RSM (Reynolds Stress Model) models.

2.2.1 Turbulence Model

The RANS models assume that the variables can be divided into a mean and fluctuating part. The pressure and velocity are then expressed as .

$$U_i = \langle U_i \rangle + u_i$$

$$P_i = \langle P_i \rangle + p_i$$

where the average velocity is defined as

$$\langle U_i \rangle = \frac{1}{2T} \int_{-T}^T U_i dt$$

The decomposition of velocity and pressure inserted into Navier-Stokes equations gives

$$\frac{\partial \langle U_i \rangle}{\partial t} + \langle U_i \rangle \frac{\partial \langle U_i \rangle}{\partial x_j} = -\frac{1}{\rho} \frac{\partial}{\partial x_j} \left\{ \langle P \rangle \delta_{ij} + \mu \left(\frac{\partial U_i}{\partial x_j} + \frac{\partial U_j}{\partial x_i} \right) - \rho \langle u_i u_j \rangle \right\} \quad (2.7)$$

The last term $-\rho \langle u_i u_j \rangle$ is called the Reynolds stresses and describes the velocity fluctuations caused by turbulence. This term needs to be modeled to close this equation.

The Reynolds averaged stress models use the Boussinesq approximation which is based on the assumption that the Reynolds stresses are proportional to mean velocity gradient. The Boussinesq approximation assumes that the eddies behave like the molecules, that the turbulence is isotropic and that the stress and strain are in local equilibrium. These assumptions cannot be made for certain flows, e.g., the highly swirling flows having a large degree of anisotropic

turbulence and then inaccurate results are obtained. The Boussinesq approximation allows the Reynolds stresses to be modeled using a turbulent viscosity which is analogous to the molecular viscosity[17]. Thus above equation becomes,

$$\frac{\partial \langle U_i \rangle}{\partial t} + \langle U_j \rangle \frac{\partial \langle U_i \rangle}{\partial x_j} = -\frac{1}{\rho} \frac{\partial \langle P \rangle}{\partial x_i} - \frac{2}{3} \frac{\partial k}{\partial x_i} + \frac{\partial}{\partial x_j} \left[(\nu + \nu_T) \left(\frac{\partial U_i}{\partial x_j} + \frac{\partial U_j}{\partial x_i} \right) \right] \quad (2.8)$$

The use of RANS models requires that two additional transport equations, for the turbulence kinetic energy, k , and the turbulence dissipation rate, ε , or the specific dissipation rate, ω , are solved.

2.2.2 Two-Equations Models

Different turbulence models can be classified on the basis of number of extra equations used to close the set of equations. There are zero, one and two equations models which are commonly employed for turbulence modeling. Zero equation model makes a simple assumption of constant viscosity (Prandtl's mixing length model). Whereas one equation model assumes that viscosity is related to history effects of turbulence by relating to time average kinetic energy. Similarly, two equation model uses two equations to close the set of equations. These two equations can model turbulent velocity or turbulent length scales. There are many variables which can be modeled for example vorticity scale, frequency scale, time scale and dissipation rate. Among these variables, dissipation rate ε is the most commonly used variable. This model is named with respect to the variables being modeled. For example $k - \varepsilon$ model, as it models k (Turbulent kinetic energy) and $k - \varepsilon$ (Turbulent energy dissipation rate). Another, important turbulence model is $k - \omega$ model. It models k (Turbulent kinetic energy) and ω (Specific dissipation rate). These models have become now common in industrial use. These provide significant amount of reliability as they use two variables to close the set of equations[18].

$k - \varepsilon$ Models

The first transported variable is turbulent kinetic energy, k . The second transported variable in this case is the turbulent dissipation, ε . Their respective modeled transport equations are as under,

For k ,

$$\frac{\partial k}{\partial t} + \langle U_j \rangle \frac{\partial k}{\partial x_j} = \nu_T \left[\left(\frac{\partial \langle U_i \rangle}{\partial x_j} + \frac{\partial \langle U_j \rangle}{\partial x_i} \right) \frac{\partial \langle U_i \rangle}{\partial x_j} \right] - \varepsilon + \frac{\partial}{\partial x_j} \left[\left(\nu + \frac{\nu_T}{\sigma_k} \right) \frac{\partial k}{\partial x_j} \right]$$

And for ε

$$\frac{\partial \varepsilon}{\partial t} + \langle U_j \rangle \frac{\partial \varepsilon}{\partial x_j} = C_{\varepsilon 1} \nu_T \frac{\varepsilon}{k} \left[\left(\frac{\partial \langle U_i \rangle}{\partial x_j} + \frac{\partial \langle U_j \rangle}{\partial x_i} \right) \frac{\partial \langle U_i \rangle}{\partial x_j} \right] + C_{\varepsilon 2} \frac{\varepsilon^2}{k} + \frac{\partial}{\partial x_j} \left[\left(\nu + \frac{\nu_T}{\sigma_\varepsilon} \right) \frac{\partial \varepsilon}{\partial x_j} \right]$$

The physical interpretation of the ε equation is,

1. Accumulation of ε
2. Convection of ε by the mean velocity
3. Production of ε

4. Dissipation of ε

5. Diffusion of ε

The time constant for turbulence is calculated from the turbulent kinetic energy and dissipation rate of turbulent kinetic energy.

$$\tau = \frac{k}{\varepsilon}$$

Note that the source term in ε equation is same as in the k -equation divided by the time constant τ and the rates of dissipation ε is proportional to $\frac{\varepsilon}{\tau} = \frac{\varepsilon^2}{k}$.

The turbulent viscosity must be calculated to close the $k - \varepsilon$ model. As the turbulent viscosity is given as the product between characteristic length and velocity scales, $\nu_T \propto ul$. This means that, $\nu_T = C_\mu \frac{k^2}{\varepsilon}$.

Finally five closure coefficients are considered to be constant for all flows, though they can change a little from one flow to the other[17]. The values for these closure coefficients are given in the Table below.

Table 2.1: Closure Coefficients for $k - \varepsilon$ Model

Constant	Value
C_μ	0.09
$C_{\varepsilon 1}$	1.44
$C_{\varepsilon 2}$	1.92
σ_k	1.00
σ_ε	1.30

The standard $k - \varepsilon$ model does not always give good results. There are some flows which cannot be predicted accurately, such as streamline curvature, swirling flows and axis-symmetrical jets. The inaccuracies stem from underlying Boussinesq hypothesis which imposes isotropy and the way it models the dissipation equation. This model was derived and tuned for high Reynolds numbers. This implies that it is suited for flows where the turbulence is nearly isotropic and to flows where energy cascade proceeds in local equilibrium with respect to generation. Furthermore, the model parameters in $k - \varepsilon$ model are a compromise to give a best performance for wide range of different flows. Due to these weaknesses in $k - \varepsilon$ model, several variants are derived for overcoming some of its shortcomings. Realizable $k - \varepsilon$ model is one of them and is described here.

Realizable $k - \varepsilon$ Model

The realizable $k - \varepsilon$ model differs from the standard $k - \varepsilon$ model in that it features a realizability constraint on the predicted stress tensor, thereby giving the name of realizable $k - \varepsilon$ model. The difference comes from correction of the k -equation where the normal stress can become negative in the standard $k - \varepsilon$ model for flows with large strain rate. This can be seen in the normal components of the Reynolds stress tensor.

$$\langle u_i u_i \rangle = \sum_i \langle u_i^2 \rangle = \frac{2}{3}k - 2\nu_T \frac{\partial \langle U_i \rangle}{\partial x_j} \quad (2.9)$$

Note that $\langle u_i u_i \rangle$, must be larger than zero by definition since it is a sum of squares. However, equation 2.9 implies that if strain is sufficiently large, normal stresses become negative. The realizable $k - \varepsilon$ model uses a variable C_μ so that this will never occur. In fact, C_μ is no longer

constant, instead it is a function of the local state of flow to ensure that the normal stresses are positive under all flow conditions, i.e. to ensure that normal stresses are positive under all flow conditions. Realizability also means that the stress tensor satisfies $\langle u_i^2 \rangle \langle u_j^2 \rangle - \langle u_i u_j \rangle^2 \geq 0$, i.e. the Schwartz's inequality is fulfilled. Hence, the model is likely to provide better performance for flows involving rotation and separation. It is noteworthy that the realizable model is better suited to flows where the strain rate is large. This includes the flows with strong streamline curvature and rotation. Validation of complex flows, e.g. boundary layer flows, separated flows and rotating shear flows show that the realizable $k - \varepsilon$ model performs better than the standard $k - \varepsilon$ model[17][18].

$k - \omega$ SST Model

It has been a problem to accurately predict the flow separation. It is seen that standard model usually predicts the separation too late and length of separation is not accurately predicted. For this reason, near wall region becomes very important and critical in such situations. The $k - \omega$ SST turbulence model is a two equation model. This model is known because it uses both $k - \omega$ and $k - \varepsilon$ models. In a simple $k - \omega$ model, specific dissipation energy is modeled along with turbulent kinetic energy.

The modeled equation for k is as under.

$$\frac{\partial k}{\partial t} + \langle U_j \rangle \frac{\partial k}{\partial x_j} = \nu_T \left[\left(\frac{\partial \langle U_i \rangle}{\partial x_j} + \frac{\partial \langle U_j \rangle}{\partial x_i} \right) \frac{\partial \langle U_i \rangle}{\partial x_j} \right] - \beta k \omega + \frac{\partial}{\partial x_j} \left[\left(\nu + \frac{\nu_T}{\sigma_k} \right) \frac{\partial k}{\partial x_j} \right] \quad (2.10)$$

and the modeled equation for ω is

$$\frac{\partial \omega}{\partial t} + \langle U_j \rangle \frac{\partial \omega}{\partial x_j} = \alpha \frac{\omega}{k} \nu_T \frac{\varepsilon}{k} \left[\left(\frac{\partial \langle U_i \rangle}{\partial x_j} + \frac{\partial \langle U_j \rangle}{\partial x_i} \right) \frac{\partial \langle U_i \rangle}{\partial x_j} \right] - \beta^* \omega^2 + \frac{\partial}{\partial x_j} \left[\left(\nu + \frac{\nu_T}{\sigma_\omega} \right) \frac{\partial \omega}{\partial x_j} \right] \quad (2.11)$$

The turbulent viscosity can be estimated from $\nu_T = \frac{k}{\omega}$. This model is superior to standard models in a way that it models the region of low turbulence better where turbulent kinetic energy and dissipation energy both approach to zero. Whereas, the $k - \omega$ model is good in near wall regions and doesn't need the wall functions. Thus this model performs good in viscous sublayer. Due to this, it demands very fine mesh near wall, such that first grid is kept at a $y^+ < 5$. Closure coefficients for $k - \omega$ model can be seen in Table 2.2.2.

Table 2.2: Closure Coefficients for $k - \omega$ Model

Constant	Value
α	5/9
β	3/40
β^*	9/100
σ_k	1/2
σ_ω	1/2

SST models stands for Shear Stress Transport model, it is the combination of $k - \omega$ and $k - \varepsilon$ models. As $k - \varepsilon$ is a high Reynolds number model thus in the near wall region $k - \omega$ model is used. Whereas, in the region away from the walls, $k - \varepsilon$ model is used. The SST model uses a blending function whose value depends upon the distance from the walls. Near the wall, in viscous sublayer, this blending function is one and only $k - \omega$ model is used. The regions away from the wall this function is zero and uses only $k - \varepsilon$ model. This model also includes the cross diffusion term. In this model turbulent viscosity is changed to include the effect of

turbulent shear stress transport. Modeling constants are also different from other models. These characteristics make the SST model reliable for the adverse pressure gradient flows and boundary layer separation. Details can be seen in the Fluent user guide [19].

2.3 Wall Treatment Methods

The near-wall modeling considerably effects the reliability of numerical solutions, because walls are the major cause of mean vorticity and turbulence. Near the wall, gradients of variable such as velocity and pressure are high and other scalar variables also undergo sudden increase or decrease. So, precise estimation of flow variables in these regions is of major concern, which will lead to good predictions of turbulence as well.[19].

It is known that the region near wall can be divided into three sub sections. The section/layer next to the wall is named as viscous sub-layer. The flow in this layer is entirely laminar and molecular viscosity is major factor in calculating the heat and momentum transfer. In this region turbulent viscosity assumption is not valid at all. While, the section farthest from the wall inside the near wall region, is called the fully turbulent layer. Here the assumption of turbulent viscosity is valid and turbulence has a major effect over the heat and momentum transport. Then there is a transition region in between these two sections called buffer layer. In this layer, both molecular and turbulent viscosity is important[19].

Modeling of the near wall region can be achieved by fully resolving the region all the way to the wall. This approach may need very fine mesh near the wall and would definitely need huge computational resources to solve. There is another approach, in which near wall region is not resolved completely and empirical formulas are used to guess the variables at the wall. These empirical formulas are called the wall functions. Wall functions are applied on a point away from the wall outside the viscous sublayer. These wall functions are used to connect the turbulent regions with the viscous sublayer[19]. Graphical representation of these both methods can be seen in the Figure 2.1.

2.3.1 Wall Functions

Wall functions are a set of empirical formulas which connects the different variables such as velocity, temperature and pressure at the wall to the near wall region (Turbulence boundary layer). Wall functions are applied by using the law of wall for the variables near the wall region. Then they formulate the turbulence variables such as turbulent kinetic energy and turbulent dissipation energy. These formulations depend upon the respective turbulence model. There are following types of wall functions mostly used.

- Standard Wall Functions
- Non-Equilibrium Wall Functions
- Enhanced Wall Functions

Standard Wall Functions

Wall functions basically do not resolve the boundary layer. Thus in their true sense, these are not exact solution to any problem. Wall functions make it possible to calculate the boundary condition away from the wall. Use of wall functions permit the solution at a point where wall functions are suitable, rather than on the wall itself. The boundary conditions are then used at this point and wall functions compute the rapid variation of the flow variables which arise in close proximity to the wall region to be accounted for without resolving the viscous layer next

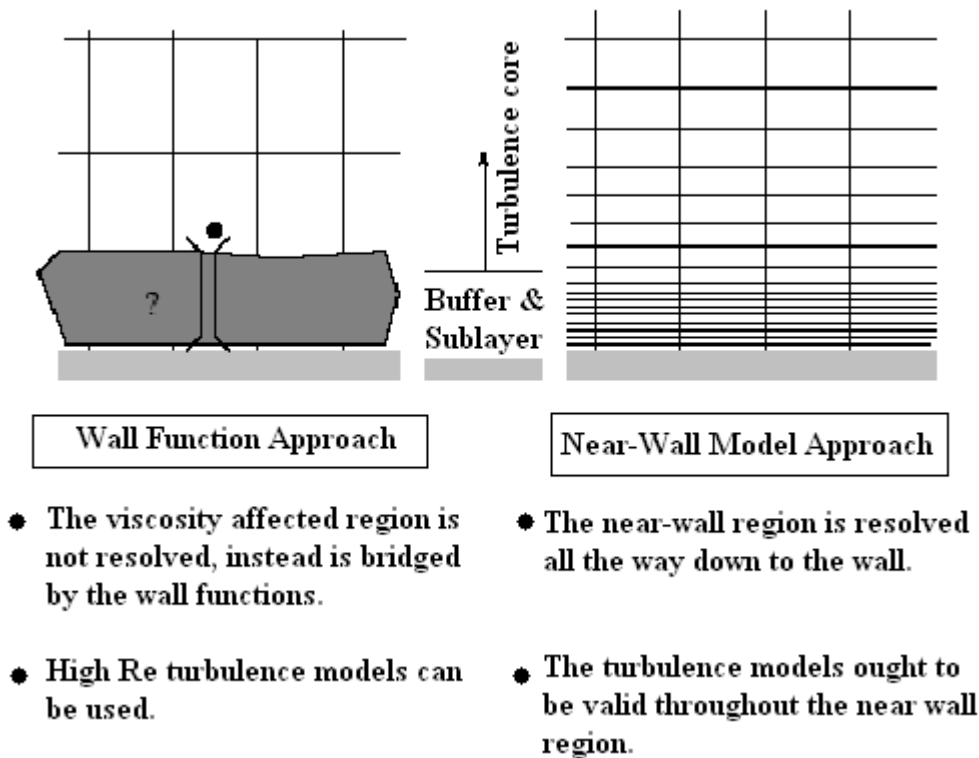


Figure 2.1: Wall Functions and Near Wall Treatment (Adopted from "Computational Fluid Dynamics for Chemical Engineers")

to wall region. Furthermore, wall functions preclude the need to modify the turbulence model to explain for viscosity layer near the wall region. The average velocity in the interior region of the boundary layer can be devised on the general form in Equation 2.12.

$$\langle U \rangle^+ = f(y^+) \quad (2.12)$$

Assuming that the total stress is constant and the turbulent part of the total stress tensor is negligible in the viscous sublayer,

$$\frac{\tau_w}{\rho} = \nu \frac{d\langle U_x \rangle}{dy} \quad (2.13)$$

Integrating with respect to y and applying the no slip boundary conditions gives

$$\langle U_x \rangle = \frac{\tau_w y}{\rho \nu} = \frac{u_w^2 y}{\nu} \quad (2.14)$$

or in the dimensionless form

$$\langle U_x \rangle^+ = y^+ \quad (2.15)$$

In the completely turbulent layer, the total stress tensor shrinks to $\tau_{xy} = -\langle u_x u_y \rangle$. As the shear stress is almost constant over the inner region of the boundary layer and is approximately equal to τ , we obtain

$$\tau_w = -\rho \langle u_x u_y \rangle \quad (2.16)$$

By introducing Prandtl's mixing length model and the relation, $l = Ky$, we obtain

$$\frac{\tau_w}{\rho} = -\langle u_x u_y \rangle = l^2 \left[\frac{d\langle U_x \rangle}{dy} \right]^2 = K^2 y^2 \left[\frac{d\langle U_x \rangle}{dy} \right]^2 \quad (2.17)$$

As the characteristic velocity scale for the sub-layers is given by $u_* = \sqrt{\tau_w/\rho}$. Equation 2.17 can now be written as

$$u_*^2 = K^2 y^2 \left[\frac{d\langle U_x \rangle}{dy} \right]^2 \quad (2.18)$$

Taking the square root of the both sides and integrating with respect to y we obtain the logarithmic velocity profile, which in dimensionless form reads

$$\langle U_x \rangle^+ = \frac{1}{K} \ln(y^+) + B \quad (2.19)$$

where $k \approx 0.42$ and $B \approx 5.0$ (K is Von Karman constant). Equation 2.19 is referred to as logarithmic law of wall or simply the log law. Thus in the viscous sub-layer velocity varies linearly with y^+ , whereas it approaches the log law in the buffer sub-layer as shown in Figure 2.3.1 below.

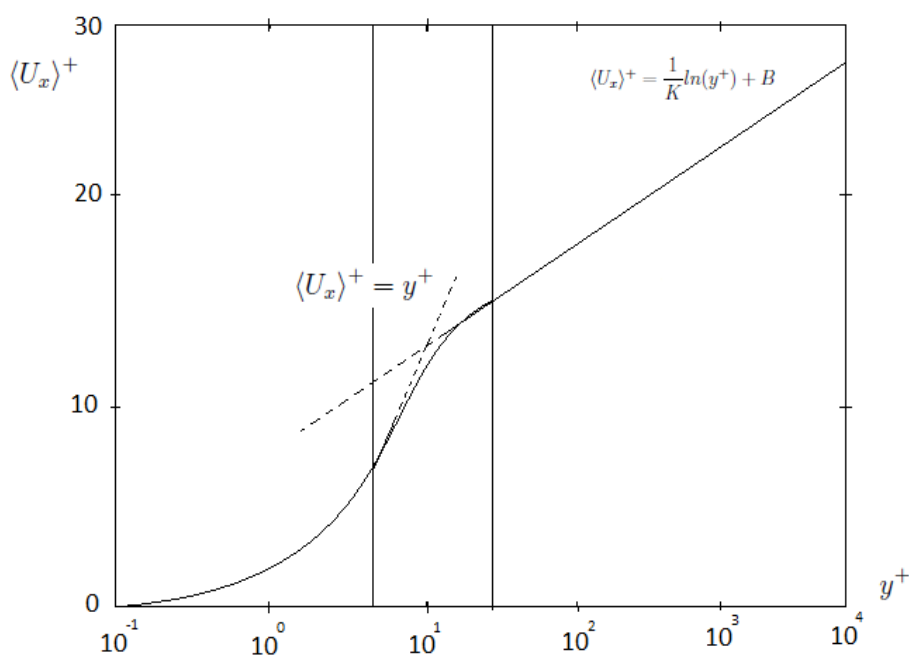


Figure 2.2: The Law of Wall (Adopted from "Computational Fluid Dynamics for Chemical Engineers")

In addition of the logarithmic profile for the average velocity, the wall functions also consists of equation for the near wall turbulent quantities. There is no transport of k to the wall while ε often has the maximum at the wall. In the derivation of boundary conditions for the turbulent quantities, it is assumed that flow is in local equilibrium which means that production equals dissipation. The boundary condition for k is given by Equation 2.20.

$$k = \frac{u_*^2}{C_\mu^{1/2}} \quad (2.20)$$

and for ε by,

$$\varepsilon = \frac{u_*^3}{k y} \quad (2.21)$$

The use of wall functions requires that the first grid point adjacent to the wall is within the logarithmic region. In dimensionless distance, that is $30 < y^+ < 100$. Upper limit of y^+ can be

as high as 300 but it should not exceed 300. Thus it can be said that use of standard wall functions requires y^+ values between 30 and 300. The log-law has proven very useful as a universal for the inner region of the flat plate turbulent boundary layer and has been experimentally verified in numerous studies. However, wall functions are not as valid under the conditions of strong pressure gradients, separated and impinging flows. In these situations standard wall functions are not appropriate choice[19].

Non-equilibrium Wall Functions

Non equilibrium wall functions are commonly used for the non-equilibrium turbulent boundary conditions. In such conditions assumption of local equilibrium between production and dissipation is not valid. Standard wall functions are based on this primary assumptions, thus limiting their use in these conditions. In boundary layer experiencing an adverse pressure gradient, the fluid closest to the wall is retarded due to the pressure increase in the stream wise direction. As a result, wall shear stress is decreased. Consequently, adverse pressure gradients alter the mean velocity profile as well as the turbulence in the boundary layer. This means that when the pressure gradient is high, the logarithmic boundary layer representation cannot be used. Hence, several flows e.g flow separation, reattachment, strong pressure gradients and flow impinging on a wall, the flow situation departs significantly from the ideal conditions and accuracy of the standard wall functions is low.

Modified wall functions which are capable to some extent in accounting for effects of pressure gradients and departure from equilibrium have been developed. By using such modified wall functions, for non-equilibrium boundary layers, improved predictions can be obtained. These wall functions typically consist of a log-law for the mean velocity, which is sensitized to pressure gradients effects. Boundary conditions for the turbulence quantities are derived based on methods where equilibrium condition is relaxed. Thus, these modifications further extend the applicability of the wall function approach and allows improvements to be obtained for complex flow conditions.

When the near wall region is of particular interest and the conditions are very non-ideal, it may be necessary to resolve the viscosity affected near wall region in detail. Such simulations, require dense meshes and modifications of high Reynolds number model since they are not valid in the near wall region[19].

Enhanced Wall Treatment

Improved modeling of wall bounded flows can be achieved using a two layer zonal approach or sing Low Reynolds number turbulence models. These techniques permit governing equations to be solved all the way to the wall, thereby eliminating the use of wall functions. It improves the predictions of wall shear stress and wall heat transfer. Resolution of the near wall region including the viscous sub-layer requires a very fine near wall grid resolution. Hence this modeling approach requires larger computational power compared to the wall function approach[19].

Two Layer Zonal Modeling

In the two layer zonal approach, the domain is divided into two zones or regions as the name implies. These two regions may be identified by the wall distance based Reynolds number.

$$Re_y = y \frac{\sqrt{k}}{\nu} \quad (2.22)$$

where y is the distance to the nearest wall.

The fully turbulent region is normally taken as $Re_y > 200$ and the viscosity affected region as

$Re_y < 200$. In the viscosity affected near wall region, a one equation turbulence model for the turbulent kinetic energy is applied and an algebraic relationship is used to calculate the energy dissipation rate. Whereas, a two-equation model such as standard or an advanced $k - \varepsilon$ model is used in the completely turbulent region. Thus, in the viscous zone the energy dissipation is calculated from,

$$\varepsilon = \frac{k^{3/2}}{l_\varepsilon} \quad (2.23)$$

where l_ε is an appropriate length scale.

It is common practice to use a blending function to calculate the viscosity in the transition region. This function simply blends the turbulent viscosity in the viscosity affected region with the turbulent viscosity in turbulent region to obtain a smooth transition. Thus blending function is defined as unity far from the wall and zero at the wall. The two layer zonal approach requires approximately the same boundary layer resolution as the low Reynolds number approach. Since the dissipation energy is calculated from an algebraic equation, this approach may be more stable compared to the low Reynolds number approach[19].

Low Reynolds Number Turbulence Models

One way of characterizing a turbulence model is to distinguish between high and low Reynolds number models. In the former, wall functions are used to approximate the turbulence quantities near the walls. The standard $k - \varepsilon$ model is an example of high Reynolds number model. These models are not valid near the wall region. Low Reynolds number models are examples of the models which are also valid in the viscous wall region and can thus be integrated all the way to the wall.

The low Reynolds number modifications typically consist of dampening functions for the source terms in the transport equation for ε and in the expression for turbulent viscosity. These modifications allow the equations to be integrated through the turbulent boundary layer, including the viscous sub-layer, thereby giving better prediction for near wall flows. It is important to point out that these models are applicable for high global Reynolds numbers. For that a transition model is needed. It should also be noted that these models are of ad-hoc nature and cannot be relied upon to give consistently good results for all type of flows. Examples of low Reynolds number variants of $k - \varepsilon$ model are the Launder-Sharma, Lam-Bremhorst and several other models.

For low Reynolds number models, the general transport equations for k are given by Equation 2.24

$$\frac{\partial k}{\partial t} + \langle U_j \rangle \frac{\partial k}{\partial x_j} = \frac{\partial}{\partial x_j} \left\{ \left(\nu + \frac{\nu_t}{\sigma_k} \right) \frac{\partial k}{\partial x_j} \right\} + \nu_t \left\{ \left(\frac{\partial \langle U_i \rangle}{\partial x_j} + \frac{\partial \langle U_j \rangle}{\partial x_i} \right) \frac{\partial \langle U_i \rangle}{\partial x_j} \right\} - \varepsilon \quad (2.24)$$

and the general transport equations for ε are given by Equation 2.25.

$$\frac{\partial \varepsilon'}{\partial t} + \langle U_j \rangle \frac{\partial \varepsilon'}{\partial x_j} = \frac{\partial}{\partial x_j} \left\{ \left(\nu + \frac{\nu_t}{\sigma_\varepsilon} \right) \frac{\partial \varepsilon'}{\partial x_j} \right\} + C_{1\varepsilon} f_1 \nu_t \frac{\varepsilon'}{k} \left\{ \left(\frac{\partial \langle U_i \rangle}{\partial x_j} + \frac{\partial \langle U_j \rangle}{\partial x_i} \right) \frac{\partial \langle U_i \rangle}{\partial x_j} \right\} - C_{2\varepsilon} f_2 \frac{\varepsilon'^2}{k} + E \quad (2.25)$$

where the turbulent viscosity is calculated by

$$\nu_T = f_\mu C_\mu \frac{k_2}{\varepsilon'} \quad (2.26)$$

and the energy dissipation, ε , is related to ε' by Equation 2.27.

$$\varepsilon = \varepsilon_0 + \varepsilon' \quad (2.27)$$

The quantities ε_0 and E are defined differently for each model, ε_0 is the value of ε at the wall. The difference between these models and the standard $k - \varepsilon$ is the dampening functions f_1 and f_2 in the equation of ε and the dampening function f_μ . The dampening functions are generally written in terms of specifically defined Reynolds numbers, such as in Equations 2.28 and 2.29.

$$Re_t = \frac{k^2}{v\varepsilon} \quad (2.28)$$

and

$$Re_y = \frac{\sqrt{ky}}{v} \quad (2.29)$$

Obviously the global Reynolds number has nothing to do with the low Reynolds number turbulent models. The low Reynolds number comes from the local Reynolds number[19].

Chapter 3

CFD Analysis

Computational fluid dynamic study of the system starts with building desired geometry and mesh for modeling the domain. Generally, geometry is simplified for the CFD studies. Meshing is the discretization of the domain into small volumes where the equations are solved by the help of iterative methods. Modeling starts with defining the boundary and initial conditions for the domain and leads to modeling the entire system domain. Finally, it is followed by the analysis of the results.

3.1 Geometry

Heat exchanger geometry is built in the ANSYS workbench design module. Geometry is simplified by considering the plane symmetry and is cut half vertically. It is a counter current heat exchanger, and the tube side is built with 11 separate inlets comprising of 8 complete tubes and 3 half tubes considering the symmetry. The shell outlet length is also increased to facilitate the modeling program to avoid the reverse flow condition. In the Figure 3.1, the original geometry along with the simplified geometry can be seen.

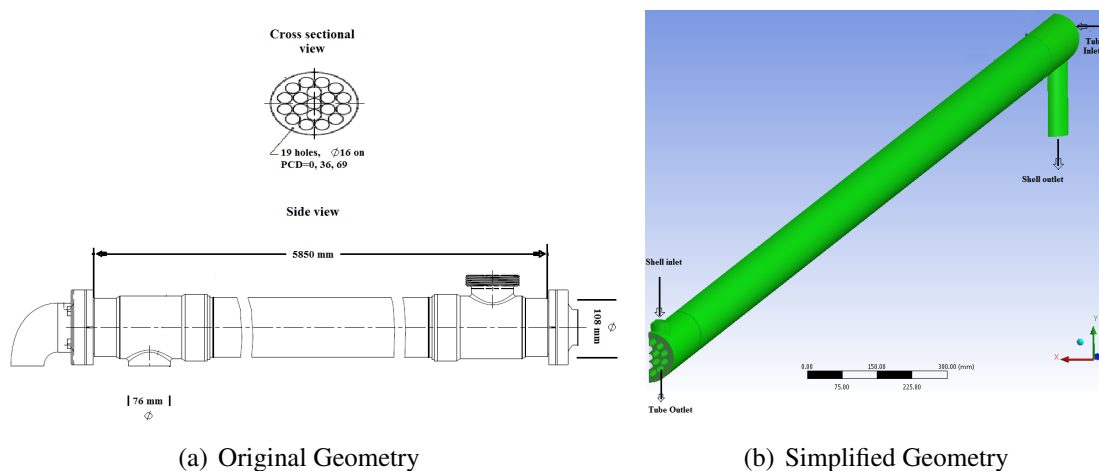


Figure 3.1: (a) and (b)

The dimensions of the geometry are also given in the Table 3.1 below.

Table 3.1: Heat Exchanger Dimensions

No.	Description	Unit	Value
1	Overall dimensions	mm	54x378x5850
2	Shell diameter	mm	108
3	Tube outer diameter	mm	16
4	Tube inner diameter	mm	14.6
5	Number of tubes		19
6	Shell/Tube length	mm	5850
7	Inlet length	mm	70
8	Outlet length	mm	200

3.2 Mesh

Initially a relatively coarser mesh is generated with 1.8 Million cells. This mesh contains mixed cells (Tetra and Hexahedral cells) having both triangular and quadrilateral faces at the boundaries. Care is taken to use structured cells (Hexahedral) as much as possible, for this reason the geometry is divided into several parts for using automatic methods available in the ANSYS meshing client. It is meant to reduce numerical diffusion as much as possible by structuring the mesh in a well manner, particularly near the wall region. Later on, for the mesh independent model, a fine mesh is generated with 5.65 Million cells. For this fine mesh, the edges and regions of high temperature and pressure gradients are finely meshed.

3.2.1 y^+ Values

y^+ values play an important role in turbulence modeling for the near wall treatment. For this reason, inflation on the walls is created to achieve the correct values of y^+ values. Requirements for the y^+ values for different wall treatments are given in the Table 3.3 [20]. It can be seen in the Table 3.3 that y^+ required for the standard and Non-equilibrium wall functions is high.

The tubes inside the shell are very close to each other and thus has very little space in between. In order to resolve the boundary layer sufficiently, 10 to 15 cells are required between the adjacent tube walls. The inflation is thus kept very fine with first cell $y^+ < 5$. This y^+ condition puts a restriction thus limiting the use of standard and non-equilibrium wall functions. For all other walls of the heat exchanger, y^+ values are set according to the wall treatment methods requirements. So when using Standard and Non-equilibrium wall functions y^+ values are less than 5 at the tube walls and at all other walls are according to requirements mentioned in Table 3.3.

3.2.2 Grid Independence

The contours from coarser mesh and fine mesh are analyzed and it is noted that fine mesh resolves the region of high pressure and temperature gradients better as compared to coarse mesh. Thus taking care of these particular regions, coarse mesh is adapted to resolve these gradients. The criterion for adaption are temperature and pressure gradients. It is mainly refined in inlet and outlet regions to get the better estimations of pressure drop and heat transfer. Rapid mixing of hot and cold fluids is observed at the outlet, which led to refine the mesh further. Adaptions on the basis of temperature and pressure gradients are made to the mesh to get a fully grid independent model. Aspect ratio of the cells is kept same as coarse mesh because it is checked that the aspect ratio doesn't effect much. Thus finally, mesh contains 2.2 million cells. Different views of all these meshes can be seen in the Table 3.2. The mesh contained different types of cells but 80%

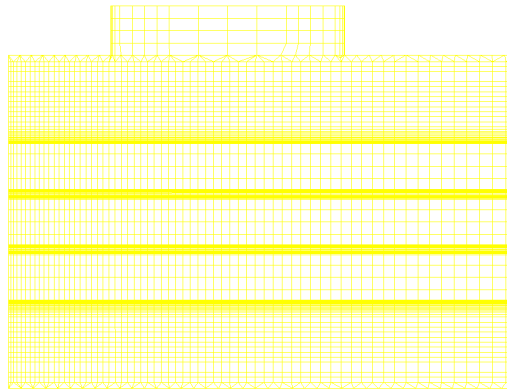
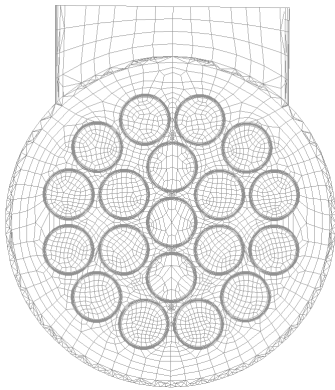
Table 3.2: Different Meshes

Mesh

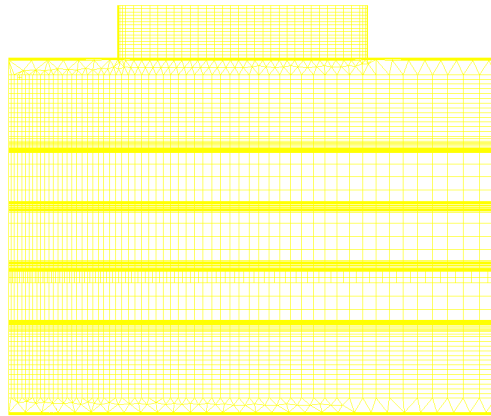
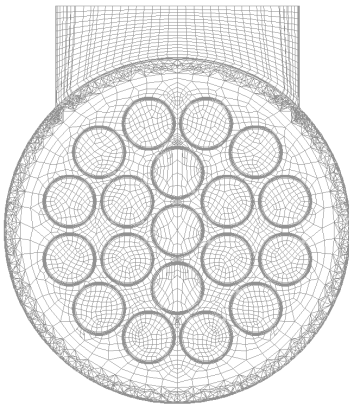
Symmetry view

Cross-section view

Coarse



Medium



Fine

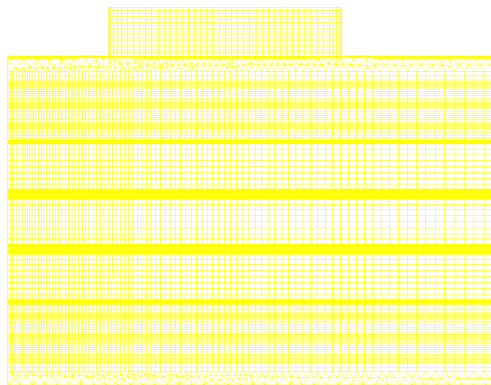
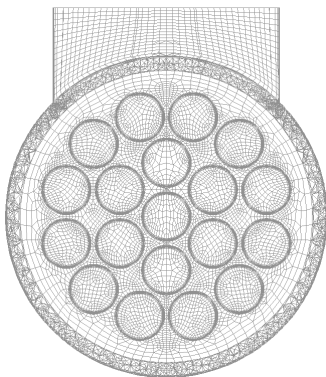


Table 3.3: y^+ Values for Different Wall Treatments

Wall Treatment Method	Recommended y^+ values	Used y^+ values at Tube walls
Standard wall functions	$30 < y^+ < 400$	$y^+ < 5$
Non-equilibrium wall functions	$30 < y^+ < 100$	$y^+ < 5$
Low Reynolds number model	$y^+ \cong 1$	$y^+ < 1$

of them are hexahedral cells. Detailed composition of the mesh can be seen in the Pi chart 3.2.2.

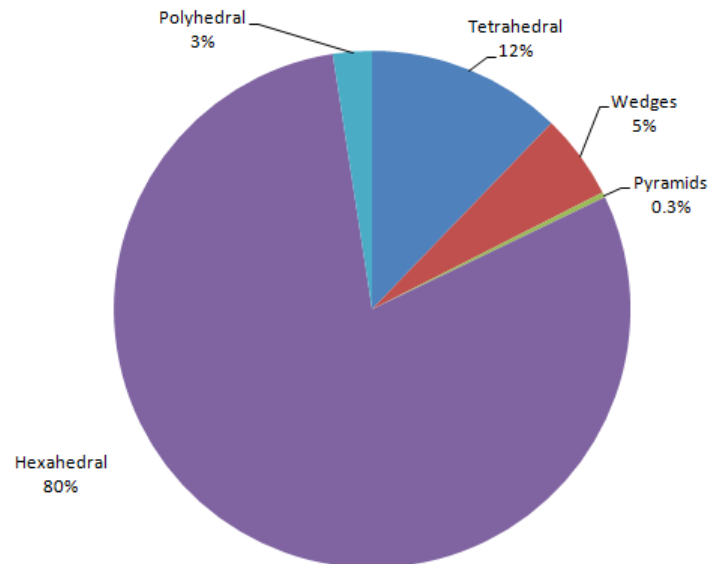


Figure 3.2: Mesh Composition

In order to see the grid independence, local velocity and temperature profiles at the shell cross-section are observed and it can be seen in Figures 3.2.2 and 3.2.2. The velocity and temperature profile for the coarse mesh is very much different from the profile obtained with Fine mesh. Thus, the coarse mesh after adaption is converted to a medium mesh of 2.2 million cells and its velocity and temperature profiles are in better agreement with fine mesh. Local heat flux depends upon temperature and mass flux (velocity of the fluid) in this case, as specific heat and density are considered constant. Thus on the basis of above mentioned results, heat flux is also found grid independent.

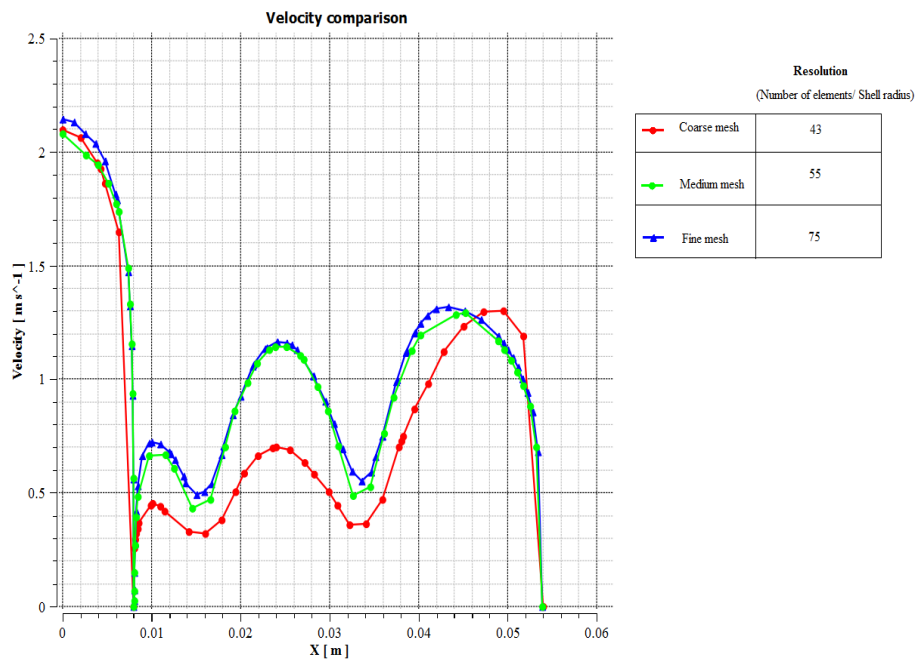


Figure 3.3: Velocity Profiles for Different Meshes

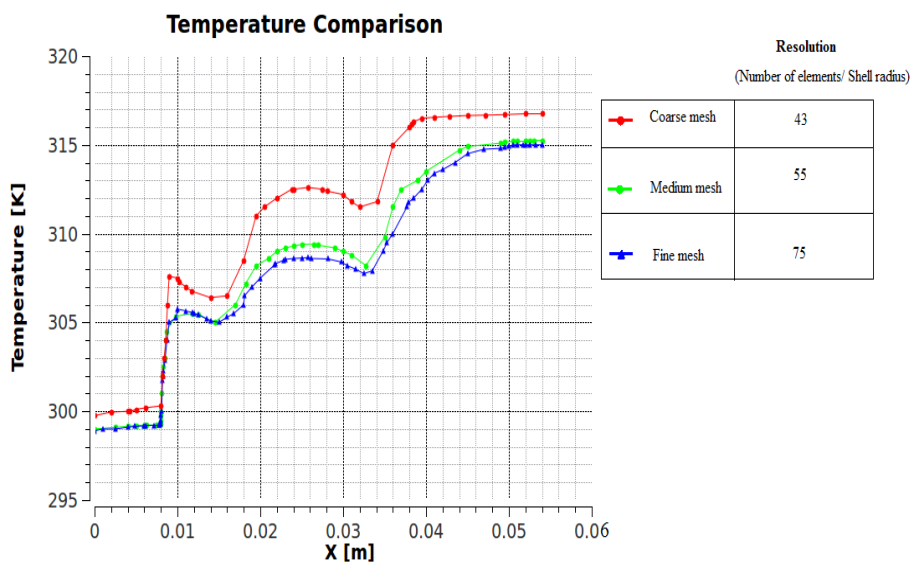


Figure 3.4: Temperature Profiles for Different Meshes

3.3 Solution

3.3.1 Boundary Conditions

Boundary conditions are used according to the need of the model. The inlet velocities and temperature are used similar to the experimental conditions in order to have a comparison. 11 tubes have 11 similar inlet and outlet boundary conditions. General correlations 3.1 and 3.2 are used to estimate the turbulence boundary conditions which are specified by estimating the turbulence intensity and length scale.

$$I = 0.16Re^{-1/8} \quad (3.1)$$

$$l = 0.07L \quad (3.2)$$

Later it is seen that the turbulence boundary conditions have a very little affect over the results and solution. The walls are separately specified with respective boundary conditions. 'No slip' condition is considered for each wall. Except the tube walls, each wall is set to zero heat flux condition. The tube walls are set to 'coupled' for transferring of heat between shell and tube side fluids. The details about all boundary conditions can be seen in the Table 3.4.

Table 3.4: Boundary Conditions

	BC Type	Shell	Tube
Inlet	Velocity-inlet	1.2 m/s	1.8 m/s
Outlet	Pressure-outlet	0	0
Wall	No slip condition	No heat flux	Coupled
Turbulence	Turbulence Intensity	3.6%	4%
	Length Scale	0.005	0.001
Temperature	Inlet temperature	317K	298K
Mass flow rate		20000kg/hr	20000kg/hr

3.3.2 Discretization Scheme

There are several discretization schemes to choose from. Initially every model is run with the first order upwind scheme and then later changed to the second order upwind scheme. It is done to have better convergence but changed to higher order scheme to avoid the numerical diffusion. It is seen that the flow is unidirectional in most of the domain. So, it is recommended to use second order schemes for strong convection. Second order upwind scheme fulfills the property of transportiveness and is more accurate than first order scheme. A major drawback of this scheme is its unboundedness which is not the case with first order scheme.

3.3.3 Measure of Convergence

It is tried to have a good convergence through out the simulations. The solution time increases if the convergence criteria is made strict. Good thing about this model is that it doesn't take too much time to converge. Thus a strict criteria is possible to get good accurate results. For this reason unscaled residuals in ANSYS Fluent which is given as in equation 3.3 are set according to Table 3.5.

$$R^\Phi = \sum_{cellsP} \left| \sum_{nb} a_{nb} \Phi_{nb} + b - a_p \Phi_p \right| \quad (3.3)$$

Here Φ is any variable, a_p is center coefficient, a_{nb} are the influence coefficients from the neighboring cells and b is the constant part of the boundary condition.

Table 3.5: Residuals

Variable	Residual
x-velocity	10^{-6}
y-velocity	10^{-6}
z-velocity	10^{-6}
Continuity	10^{-6}
Specific dissipation energy/ dissipation energy	10^{-5}
Turbulent kinetic energy	10^{-5}
Energy	10^{-9}

Chapter 4

Results and Discussion

4.1 Model Comparison

Different turbulence models are evaluated to investigate their application for our case. Each turbulence model along with different wall treatment methods is used with medium mesh (2.2 million cells). A comparison of overall heat transfer coefficient and pressure drop obtained from these models can be seen in the Figures 4.1 and 4.2 respectively. Knowing the temperatures from CFD results, Overall heat transfer coefficient is calculated from equations 1.5 1.6 and 1.7. Due to the available experimental data for comparison, only overall heat transfer coefficient is calculated. Whereas, pressure drop can easily be calculated from CFD and thus, is compared with available experimental data.

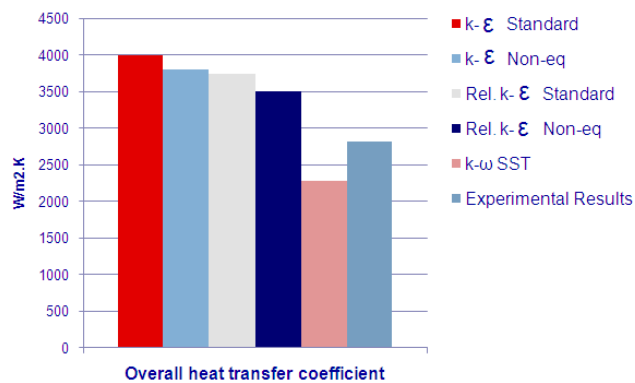


Figure 4.1: Over all Heat Transfer Coefficient

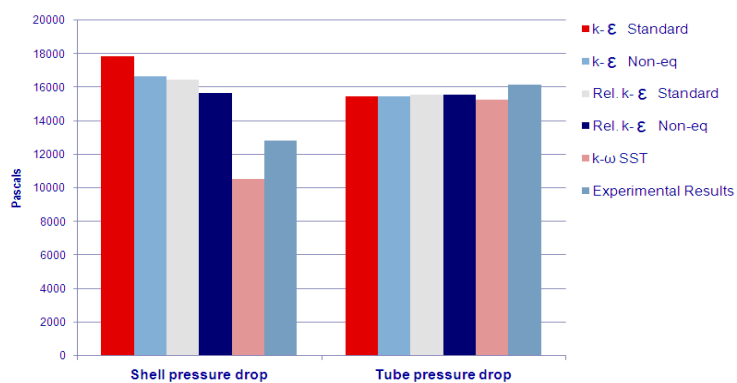


Figure 4.2: Pressure Drop

CFD results					Experimental results			% Difference		
Reynolds number $\times 10^4$		Pressure drop (kPa)		HT coefficient (W/m ² .K)	Pressure drop (kPa)		HT coefficient (W/m ² .K)	Pressure drop (kPa)		HT Coefficient (W/m ² .K)
Shell	Tube	Shell	Tube	Overall	Shell	Tube	Overall	Shell	Tube	Overall
9.2	2.16	4.04	6.01	1544.02	5.6	6.6	1965	27.91	9.0	21.4
10.64	2.52	5.32	7.99	1711.49	7.2	8.7	2196	26.16	8.2	22.1
12.16	2.88	6.8	10.3	1912.16	8.9	10.9	2414	23.63	5.7	20.8
13.68	3.24	8.41	12.7	2097.27	10.8	13.4	2621	22.14	5.3	20.0
15.2	3.6	10.5	15.2	2278.68	12.8	16.1	2819	19.69	5.7	19.2

Figure 4.3: CFD and Experimental Results

It is seen that the shell side inlet region of the heat exchanger involves boundary layer separation (adverse pressure gradient) and impinging flow on the tubes. Moreover, shell fluid's Reynolds number is found to be low in the core of the shell. Standard $k - \varepsilon$ model is used at first to get a picture of the flow distribution but it is not good for predicting the boundary layer separation and impinging flows[18]. Thus results are expected to be deviating from experimental results. Whereas, the Realizable $k - \varepsilon$ model is known for predicting the flow separation better than Standard $k - \varepsilon$. For this reason, Realizable $k - \varepsilon$ model is used with standard and then non-equilibrium wall functions. Non-equilibrium wall functions are better than standard wall functions because of their applicability in the regions of variable shear and departure from equilibrium. These wall functions also take into account the affect of high pressure gradient. The standard wall functions are over-predicting the pressure drop and heat transfer as well. Whereas, the non-equilibrium wall functions with Realizable $k - \varepsilon$ model give better results than standard $k - \varepsilon$ model. The pressure drop heat transfer still are being over-predicted by almost 25%, which is probably due to y^+ values limitations at tube walls as mentioned in Section 3.2.1 . Thus in order to avoid this and to include the low Reynold modification SST $k - \omega$ model is also used. The reason being, it uses both $k - \varepsilon$ and $k - \omega$ model in the region of high and low Reynolds number respectively.

Low Reynold number modification typically consist of dampening functions for the source terms in the transport equation for ε and in the expression for turbulent viscosity. These modifications allow the equations to be integrated through the turbulent boundary layer, including the viscous sub-layer, thereby giving better prediction for near wall flows. On the basis of above mentioned results in Figures 4.1 and 4.2, SST $k - \omega$ model is chosen for further analysis of the heat exchanger. This model is chosen because of the high global Reynolds number (i.e. in other parts of the heat exchanger away from the walls). This results in better predictions than other models and also describes the flow and temperature distributions more realistically as it would be shown in the following sections.

4.2 CFD Comparison with Experimental Results

On the basis of findings in previous Chapter, SST $k - \omega$ model with low Re modification is used with different mass flow rates to compare with experimental results. The results are given in the Figure 4.2.

The pressure drop in shell and tube side is shown in Figures 4.4 and 4.5 respectively. The pressure drop in the shell is under-predicted by the SST $k - \omega$ model by almost 20-27%. This

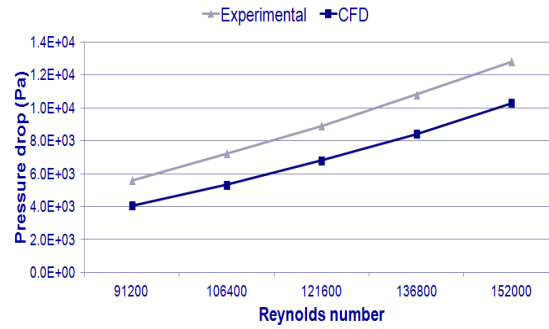


Figure 4.4: Comparison of Shell Side Pressure Drop

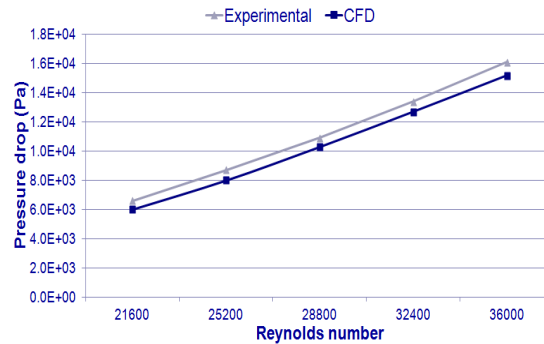


Figure 4.5: Comparison of Tube Side Pressure Drop

could be due to the several reasons including complicated geometry of the shell side and numerical diffusion. Where as, the pressure drop in tube side (straight tubes) is predicted with an average error between 5-9%. It can be due to small baffles in the tubes used in the experimental setup.

Overall heat transfer coefficient comparison with experiments can also be seen in the Figure 4.6. It is also been under-predicted by this model but still better than other models with an average error of 19-20%. The good thing about these results is the constant difference from experimental results and consistency with the real systems, i.e. with higher pressure drop, higher heat transfer is achieved.

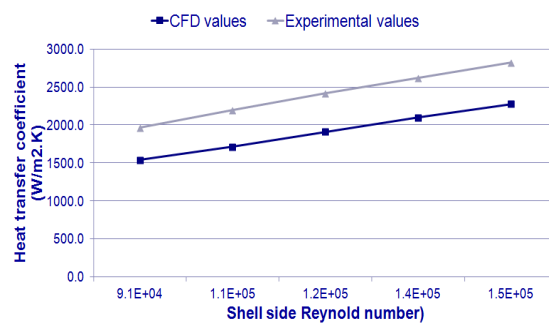


Figure 4.6: Comparison of Overall Heat Transfer Coefficient

4.3 Contour Plots

The temperature and velocity distribution along the heat exchanger can be seen through side view on the plane of symmetry. The contour plots in Figure 4.7 and 4.8 shows the whole length of heat

exchanger. The whole length is too much to be displayed on a single page with understandable resolution, thus it is cut into 4 parts to see it closely. The top most part is the inlet region and lowest part is the outlet.

As the heat exchanger is almost 6 meters long, the velocity and temperature contour plots across the cross section at different position along the length of heat exchanger will give an idea of the flow in detail. For convenience the plots are taken at 5 different positions and the details of the temperature distribution in comparison to the velocity distribution can be observed in the Table 4.1.

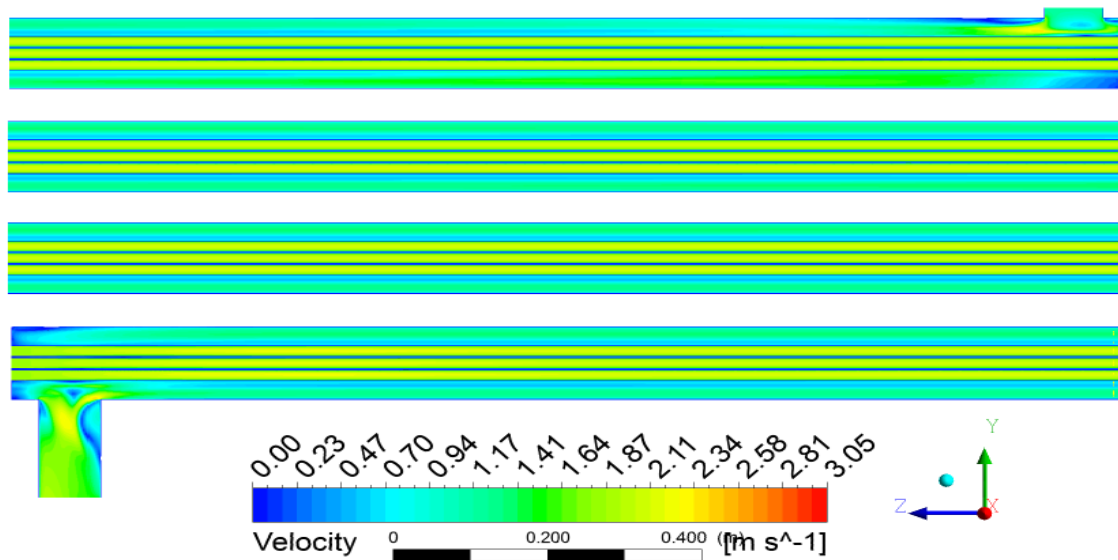


Figure 4.7: Velocity Contour Plot at Symmetrical Plane

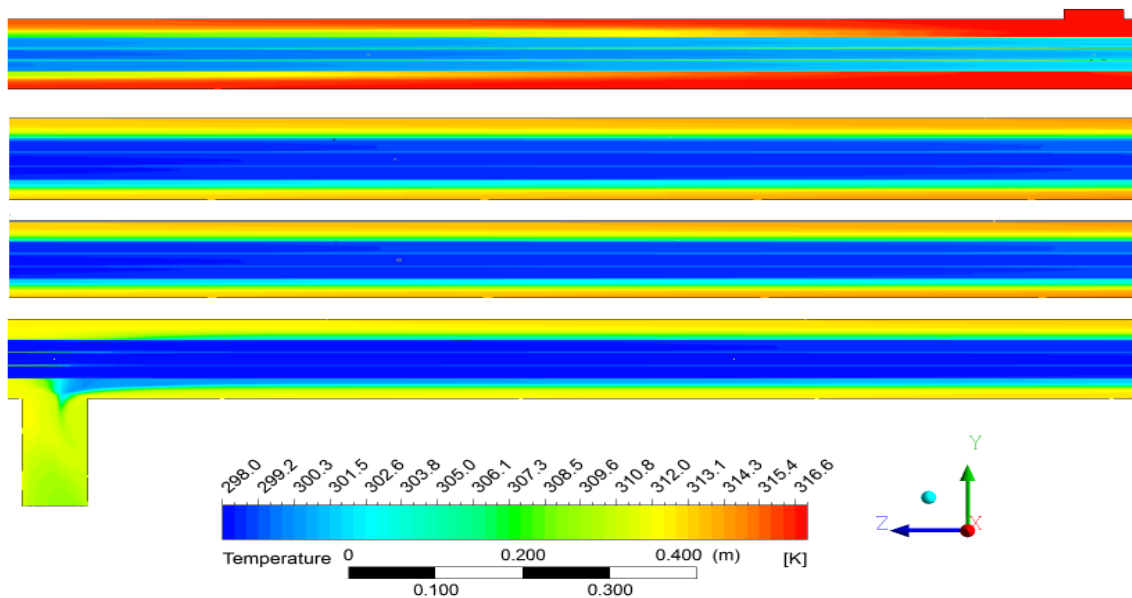
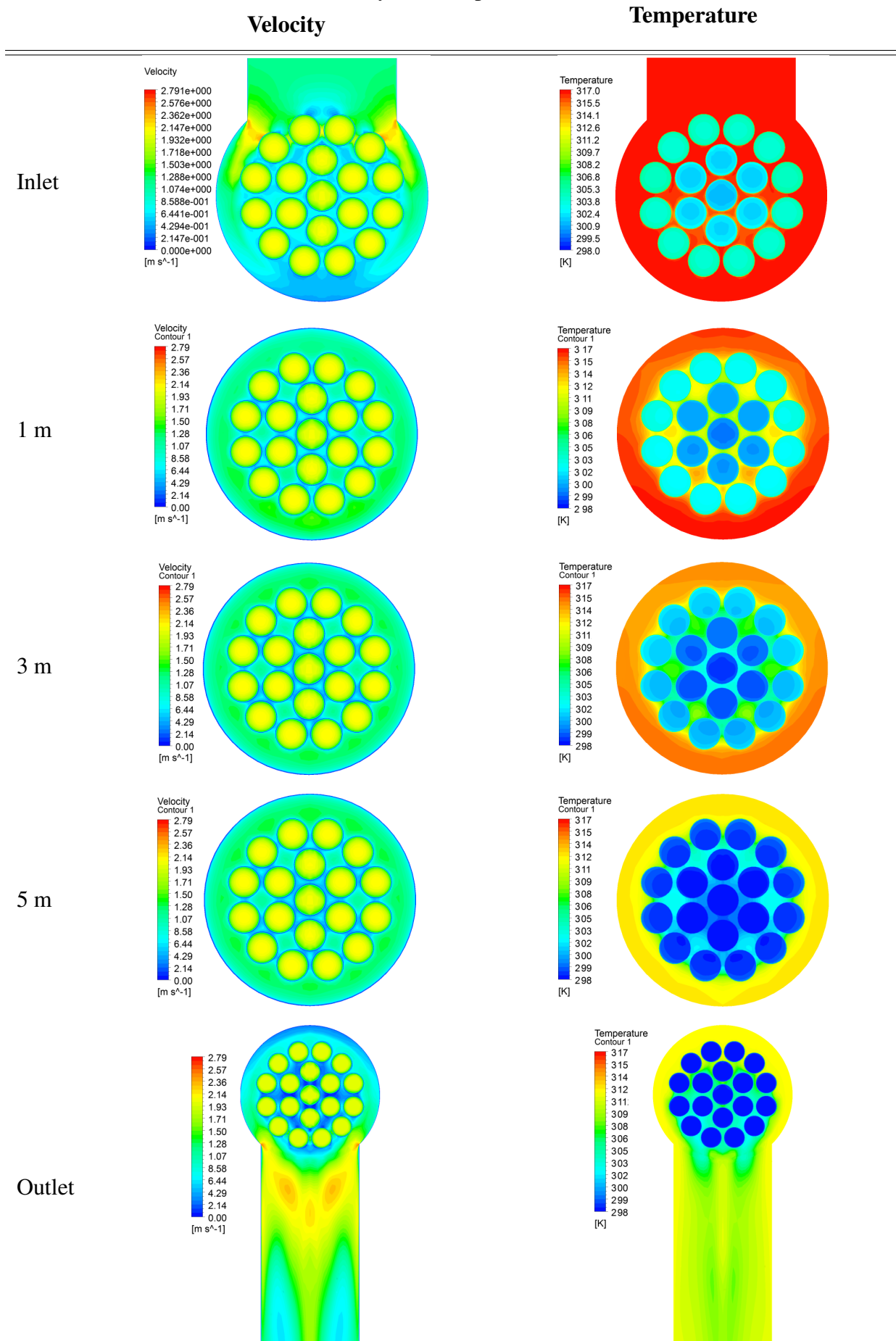


Figure 4.8: Temperature Contour Plot at Symmetrical Plane

Table 4.1: Velocity and Temperature Contour Plots



4.4 Vector Plots

Velocity vector plots can be seen below in Figures 4.9, 4.10(a) and 4.10(b). These plots give an idea of flow separation at inlet region and the impingement of the fluid on the tubes. The recirculation at the inlet region is also obvious from the Figure 4.10(b). The major portion of the fluid tends to move around the tube bundle, and part of the fluid enters the tube bundle through the tube spacing as seen in Figure 4.9. This region is a major reason of pressure drop due to impingement on the tube bundle. At the outlet, boundary layer separation takes place and the flow from the shell tends to mix with each other. This could be a non-symmetric region due to mixing of fluid from all sides.

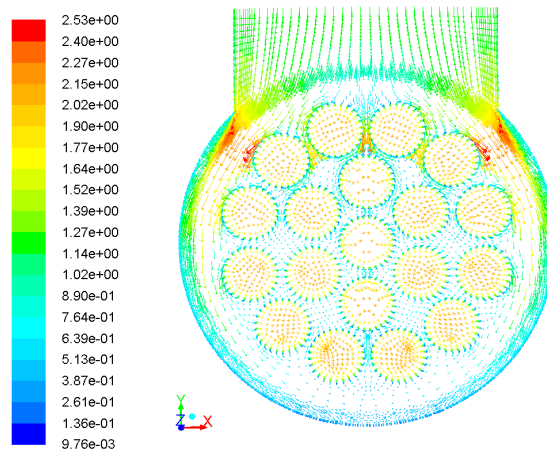


Figure 4.9: Vector Plot of Velocity at Inlet

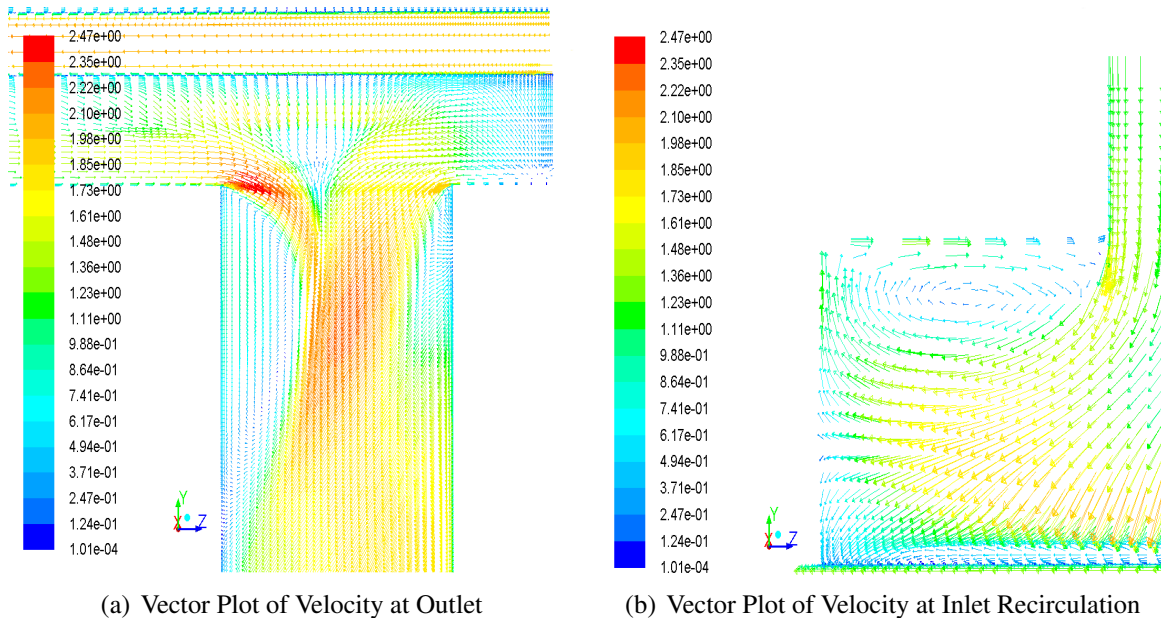


Figure 4.10: Outlet (a) and Inlet (b)

4.5 Profiles

Temperature and velocity profiles are very useful to understand the heat transfer along with the flow distribution. The temperature profiles are drawn across the cross section and along the length

of heat exchanger at different positions. Whereas, the velocity profiles are drawn only across the cross section. In order to understand the profiles, following Figures 4.11(a) and 4.11(b) must be understood first.

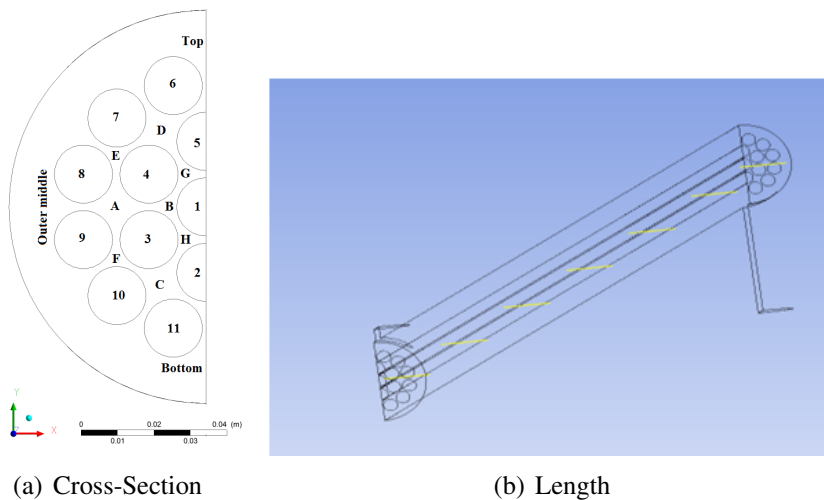


Figure 4.11: Profiling
(a) and (b)

In Figure 4.11(a), the outer edge of the shell is divided into three different names according to their positions. *Top*, *bottom* and *outer middle* can be seen in the Figure 4.11(a). Then, the inner fluid is divided into different fluid zones namely *A, B, C* to *H*. The temperature profile is drawn at these locations through to the whole length of the heat exchanger. It is done to understand their temperature profiles separately along the length of heat exchanger because the shell fluid remains parallel to tubes and doesn't mix until the outlet region. The tubes are also numbered *I* to *II*. Where *I* being the inner most tube and *6* to *II* being the outer row of tubes exposed to the outer shell fluid.

In Figure 4.11(b), the yellow lines are drawn across the cross-section (joining the circumference and center of the shell cross-section). These lines are drawn at different positions in the heat exchanger, where temperature and velocity profiles are drawn.

4.5.1 Velocity Profile

Before going into detailed discussions, velocity profile is examined to understand the flow distribution across the cross section at different positions in heat exchanger. Below in Figure 4.12 is the velocity profile. Here x-axis is the distance from the center and y-axis is the local velocity of the fluid. It should be kept in mind that the heat exchanger is modeled considering the plane symmetry. Thus the graph is showing only half the cross section of whole shell. The high peak on the left is a part of the tube side velocity, thus should not be confused with rest of the graph.

It can be seen that the velocity profile at the inlet is not consistent due to the cross flow and high pressure gradients. The flow seems to be developed as it reaches to 1 m length, and is observed to keep this profile until it reaches outlet region. Three peaks can be seen in every profile. The highest peak which is on the most right of the graph represents the outer fluid. The smallest peak represents the velocity for the fluid nearest to the inner tube. Thus at a given cross section the outer fluid is moving at higher a velocity compared to the inner fluid. It can be explained by the enhanced affect of skin friction due to the nearby tubes at the inner core of shell. It also tells that the residence time for the outer fluid is less than the inner fluid, resulting in less heat transfer.

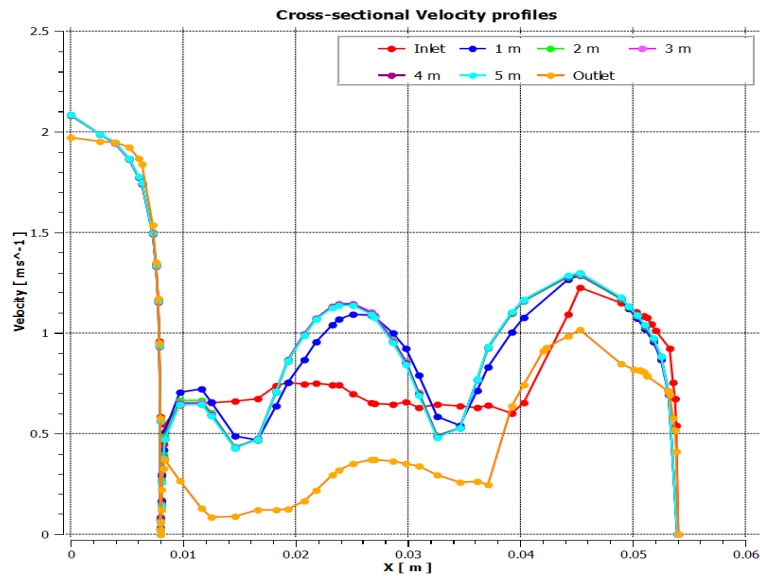


Figure 4.12: Velocity Profiles Across the Cross-section at Different Positions in the Heat Exchanger

4.5.2 Temperature Profiles

Temperature profiles in the shell and tube side can be drawn in several ways. Similar to velocity profiles, temperature is also drawn across the cross section at different positions.

Shell Side Temperature Profiles

Graph in the Figure 4.13 shows the temperature profile along the cross section of the shell according to Figure 4.11(b). The red line shows the temperature profile at the inlet, which is more or less constant. 1 meter away from inlet, temperature falls down due to heat transfer to the tubes. This fall in temperature is not same across the cross section of the heat exchanger. The peaks show the variation in shell side temperature across the cross section of shell. It is observed that the fluid near the center of the shell loses temperature much more than the fluid at the outer edge as obvious from the smallest peak near to the center and larger peak farthest from center. This trend is obeyed until outlet region of heat exchanger. At the outlet, the inner fluid tends to mix with the outer fluid and this causes a little smoothing of the temperature profile. This temperature profile alongside velocity profile provides the justification of heat transfer variation in the cross section. It is observed that the shell fluid outside the tube bundle is flowing with higher velocity, thus has lower residence time and resulting in lesser contribution in heat transfer. Whereas, the shell fluid in the core of shell is flowing with less velocity and has longer residence time and contact with the tubes, resulting in higher heat transfer.

Tube Side Temperature Profiles

Below in the Figure 4.14 are the temperature profiles for the tube side fluid along the heat exchanger. Here the x-axis is the length of heat exchanger. It shows how the fluid temperature inside the tubes rises along the length of the heat exchanger. It is clear from the profiles that the outer bundle of tubes leaves at higher temperature as compared to the inner tube bundle. Thus inner tubes are less heated and outer tubes are heated to a higher temperature. It is exactly opposite to what discussed earlier for the shell side fluid, where the outer shell fluid transfer less heat and inner shell fluid transfer more heat to the tubes. This behavior is explained later.

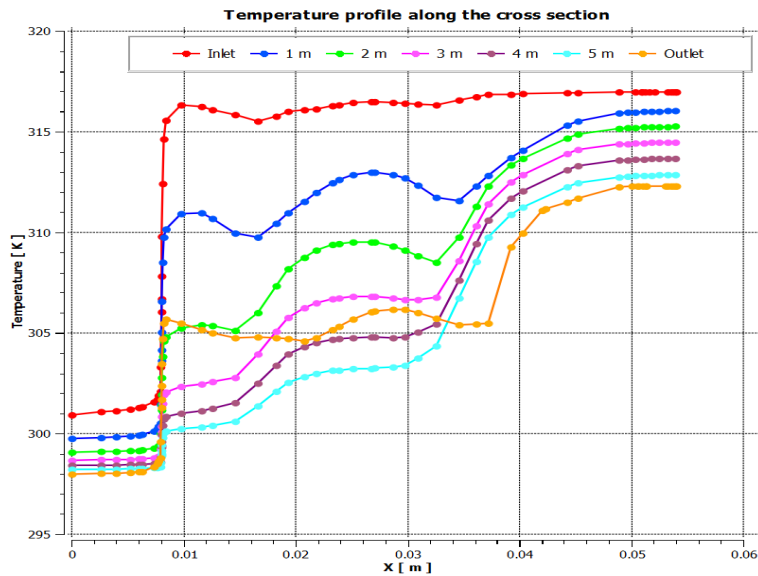


Figure 4.13: Temperature Profiles Across the Cross-section at Different Positions in the Heat Exchanger

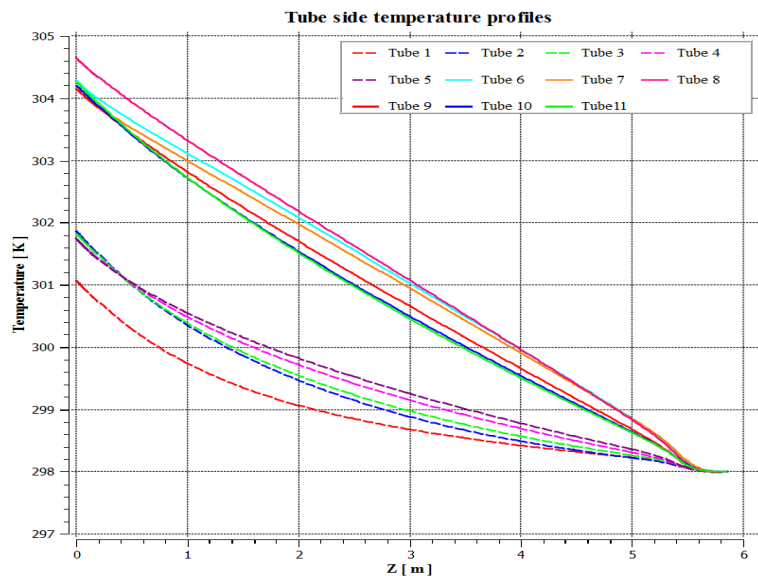


Figure 4.14: Tube side Temperature Profiles along the Length of Heat Exchanger

Mass averaged temperature of both shell and tube side along the heat exchanger can be seen in the Figure 4.15. The temperature difference remains constant.

Heat Transfer Trend

The Figure 4.16 below shows the temperature profile for the both shell side and tube side fluids.

- Temperature profile for the shell side fluid is drawn at four different positions, i.e. Top, Line B, D, and G. These positions are selected in such a way that top is farthest from the inner most tube and moving from B to G, G is the closest to the inner tube.
- As it is obvious from the previous discussion, the fluid nearest to the inner most tube i.e. G, cools down rapidly. Thus it has the largest temperature gradient until 2 meters length. But after 2 meters it becomes parallel to the top line.

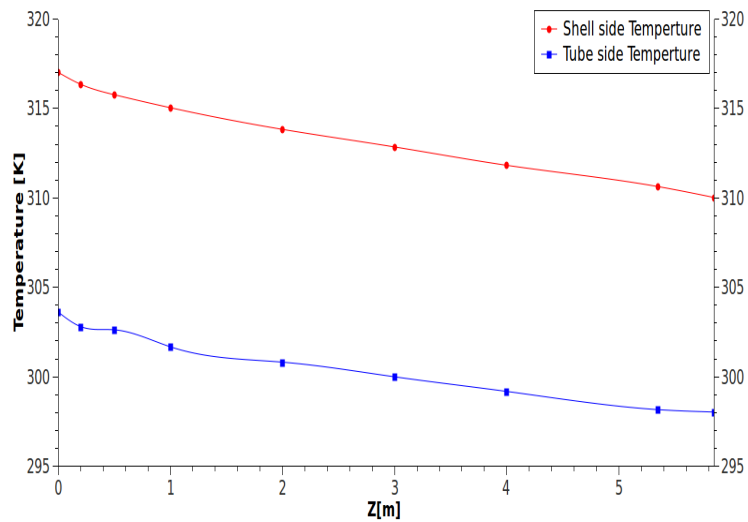


Figure 4.15: Mass Averaged Shell and Tube side Temperatures

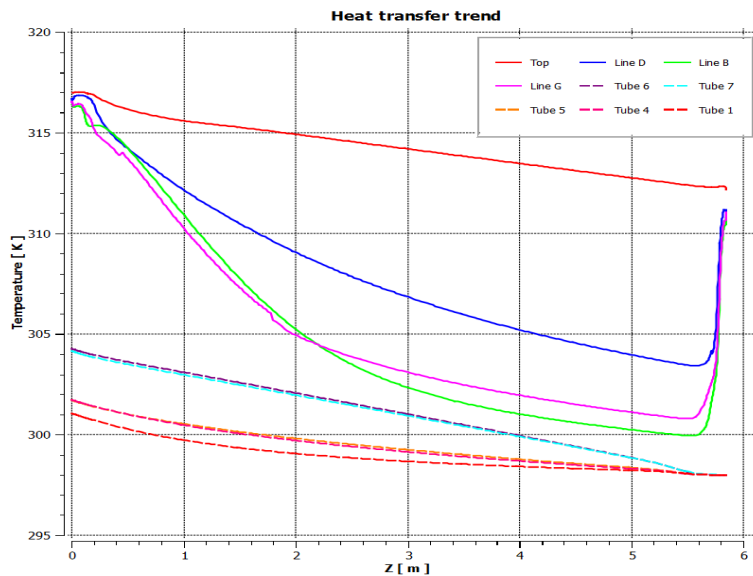


Figure 4.16: Shell and Tube Side Temperature Profiles along the Length of Heat Exchanger

- The rapid drop in shell side temperature in the beginning shows the effect of cross flow at the inlet region, which can also be observed in the tube side fluid temperature.
- Tubes 1, 4 and 5 which are inner tubes of the tube bundle, shows increase in temperature at the shell inlet region.
- Most of the heat transfer is occurring at the first 3 meter length of heat exchanger, which shows the poor usage of available heat transfer area.

4.6 Mass and Heat Flux

The velocity difference can also be explained by the help of wall distance based Reynolds number Re_w . The distribution of this Reynolds number can be observed in the contour plot in Figure 4.17(a).

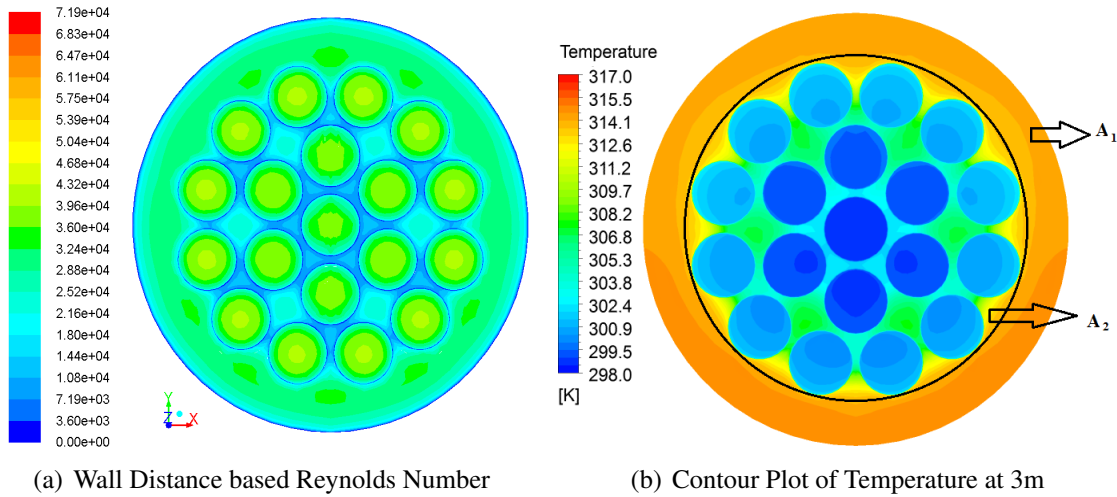


Figure 4.17: Reynolds number (a) and Temperature (b)

This contour plot depicts the situation in a better way. The flow is developed giving rise to higher Re at the outer edge of the shell. Whereas, the Reynold number is very low in the middle of the shell. This figure also alarms the fact that the most of the fluid is flowing around the tube bundle and very little flows inside. If it is assumed that fluid is divided in two sections of areas A_1 and A_2 .

$$D_2 = 86mm$$

$$D_{tot} = 108mm$$

According to Figure 4.17(b) ratio of the flow area becomes,

$$\frac{A_2}{A_{tot}} = 0.37 \cong \frac{1}{3}$$

The velocities can be taken from CFD results and mass flux integrated on the respective areas results in,

$$\frac{\text{Mass flux in the inner core}}{\text{Total mass flux}} = \frac{\int m_2 dA_2}{\int m_{tot} dA_{tot}} = 0.28 \cong \frac{1}{4}$$

The mass flux in the inner core came out to be 1/4th of the total flux, thus 3/4th is flowing around the tube bundle. This is the reason that inner tubes are heated to a lower temperature compared to outer tubes. The ratio of heat flux can give a better idea and can be calculated as followed.

$$\frac{\text{Heat flux in the inner core}}{\text{Total heat flux}} = \frac{\int m_2 C_p (T - T_{ref}) dA_2}{\int m_{tot} C_p (T - T_{ref}) dA_{tot}} = 0.37 \cong \frac{1}{3}$$

Thus from above calculation it is inferred that the inner fluid which is 25% of the total fluid is transferring 33% of the total heat transferred. Whereas, the outer fluid which is 75% of total fluid, transfers 66% of the total heat transfer. Thus outer fluid is mostly bypassing the tube bundle and needs improvement from design point of view.

4.7 Pressure Drop and Heat Transfer

Pressure drop along the length of heat exchanger can be seen in the Figure 4.18. It depicts the static pressure at inlet and outlet regions and along the length of tubes at different inlet velocities. The steeper inclination at the beginning and end of the graph shows the higher pressure drops at

inlet and outlet regions. As described earlier, this happens due to cross-flow and impingement of the flow at inlet and outlet of the heat exchanger. Subsequently, heat transfer at these regions is higher as compared to the rest of heat exchanger. It can be seen in the Figure 4.19 that local heat transfer coefficient is very high at the inlet. This is due to several reasons, mainly being the cross flow at inlet. In addition, the temperature difference between the shell side and tube side fluid is much higher as observed in Figure 4.16.

The study of both Figures 4.18 and 4.19 gives an idea of effect of cross-flow over the pressure drop and heat transfer. Certainly, creating cross-flow regions enhances the heat transfer at the cost of higher pressure drop. Thus it provides an insight about installing baffles for higher heat transfer in this thin and long heat exchanger.

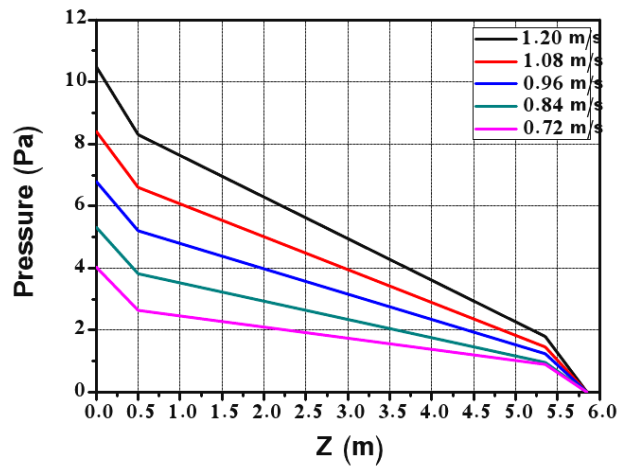


Figure 4.18: Shell Side Pressure Drop along the Length of Heat Exchanger

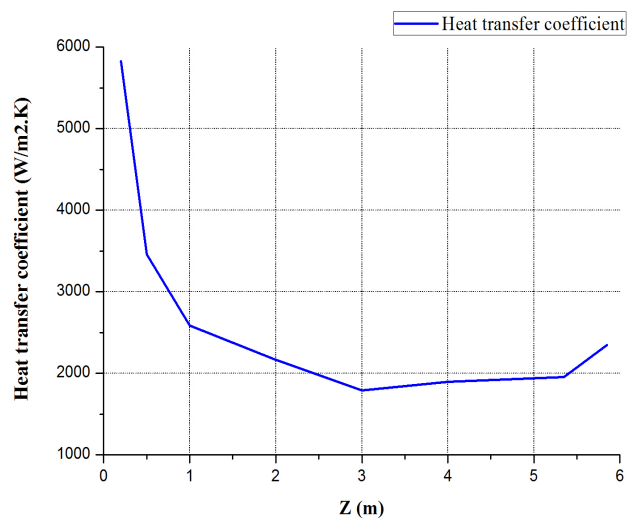


Figure 4.19: Heat Transfer Coefficient along the Length of Heat Exchanger

Chapter 5

Conclusions

The heat transfer and flow distribution is discussed in detail and proposed model is compared with the experimental results as well. The model predicts the heat transfer and pressure drop with an average error of 20%. Thus the model still can be improved. The assumption of plane symmetry works well for most of the length of heat exchanger except the outlet and inlet regions where the rapid mixing and change in flow direction takes place. Thus improvement is expected if complete geometry is modeled. Moreover, SST $k - \omega$ model has provided the reliable results given the y^+ limitations, but this model over predicts the turbulence in regions with large normal strain (i.e. stagnation region at inlet of the shell). Thus the modeling can also be improved by using Reynold Stress Models, but with higher computational costs. Furthermore, the enhanced wall functions are not used in this project due to convergence issues, but they can be very useful with $k - \varepsilon$ models.

The heat transfer is found to be poor because the most of the shell side fluid by-passes the tube bundle without interaction. Thus the design can be modified in order to achieve the better heat transfer in two ways. Either, the shell diameter is reduced to keep the outer fluid mass flux lower or tube spacing can be increased to enhance the inner fluid mass flux. Just doing this might not be enough, because it is seen that the shell side fluid after 3m doesn't transfer heat efficiently. It is because the heat transfer area is not utilized efficiently. Thus the design can further be improved by creating cross-flow regions in such a way that flow doesn't remain parallel to the tubes. It will allow the outer shell fluid to mix with the inner shell fluid and will automatically increase the heat transfer.

Bibliography

- [1] “A heat exchanger applications general.” http://www.engineersedge.com/heat_exchanger/heat_exchanger_application.htm, 2011.
- [2] S. Kakac and H. Liu, “Heat exchangers: Selection, rating, and thermal performance,” 1998.
- [3] <http://www.wcr-regasketing.com>, “Heat exchanger applications.” <http://www.wcr-regasketing.com/heat-exchanger-applications.htm>, 2010.
- [4] D. Kern, *Process Heat Transfer*. McGraw-Hill, 1950.
- [5] R. Serth, *Process Heat Transfer, Principles and Applications*. Elsevier Science and Technology Books,.
- [6] E. Ozden and I. Tari, “Shell side cfd analysis of a small shell-and-tube heat exchanger,” *Energy Conversion and Management*, vol. 51, no. 5, pp. 1004 – 1014, 2010.
- [7] J. J. Gay B, Mackley NV, “Shell-side heat transfer in baffled cylindrical shell and tube exchangers- an electrochemical mass transfer modelling technique,” *Int J Heat Mass Transfer*, vol. 19, pp. 995–1002, 1976.
- [8] G. V. Gaddis ES, “Pressure drop on the shell side of shell-and-tube heat exchangers with segmental baffles,” *Chem Eng Process*, vol. 36, pp. 149–59, 1997.
- [9] F. E. Idelchik, I.E., *Handbook of hydraulic resistance*. Hemisphere Publishing, New York, NY, second ed., 1986.
- [10] M. J. Van Der Vyver H, Dirker J, “Validation of a cfd model of a three dimensional tube-in-tube heat exchanger,,” 2003.
- [11] S. B., “Computational heat transfer in heat exchangers,” *Heat Transfer Eng*, pp. 24:895–7, 2007.
- [12] A. M. Prithiviraj M, “Shell and tube heat exchangers. part 1: foundation and fluid mechanics,” *Heat Transfer*, p. 33:799–816., 1998.
- [13] K. T. C. S. Sha WT, Yang CI, “Multidimensional numerical modeling of heat exchangers,,” *Heat Transfer*, vol. 104, pp. 417–25, 1982.
- [14] N. B. M. Bhutta, M.A.A Hayat, “Cfd applications in various heat exchangers design: A review,” *Applied Thermal Engineering*, vol. 32, pp. 1–12, 2011.
- [15] J. G. Jae-Young, K. Afshin, “Comparison of near-wall treatment methods for high reynolds number backward-facing step flow,” *Int. J Computational Fluid Dynamics*, vol. 19, 2005.
- [16] E. Cao, *Heat Transfer in Process Engineering*. McGraw Hill, 2009.

- [17] B. Andersson, R. Andersson, L. Håkansson, M. Mortensen, R. Sudiyo, and B. V. Wachem, *Computational Fluid Dynamics for Chemical Engineers*. sixth ed., 2010.
- [18] H. K. Versteeg and M. W., *An Introduction to Computational Fluid Dynamics, The Finite Volume Method*. Pearson Education Limited, 2007.
- [19] “Ansys fluent theory guide.” <http://www.ansys.com>, 2010.
- [20] “Cfd-online wiki.” http://http://www.cfd-online.com/Wiki/Main_Page, 2011.